PRESYNAPTIC CALCIUM CURRENTS IN SQUID GIANT SYNAPSE

R. LLINÁS, I. Z. STEINBERG, AND K. WALTON, *Department of Physiology and Biophysics, New York University Medical Center, New York 10016, and Department of Chemical Physics, Weizmann Institute of Science, Rehovot, Israel*

ABSTRACT A voltage clamp study has been performed in the presynaptic terminal of the squid stellate ganglion. After blockage of the voltage-dependent sodium and potassium conductances, an inward calcium current is demonstrated. Given a step-depolarization pulse, this voltage- and time-dependent conductance has an S-shaped onset. At the "break" of the voltage step, a rapid tail current is observed. From these results a kinetic model is generated which accounts for the experimental results and predicts for the time course and amplitude a possible calcium entry during presynaptic action potentials.

INTRODUCTION

Present knowledge regarding chemical synaptic transmission suggests that intracellular ionic calcium is the triggering parameter for synaptic vesicle fusion and, thus, for the subsequent transmitter release from the presynaptic element (Katz, 1969). Indeed, increase in intracellular calcium concentration, $[Ca^{2+}]_i$, has been shown to produce such release, whether by means of (*a*) voltage-dependent membrane conductance increase (Katz and Miledi, 1969a; Llinás and Nicholson, 1975), (*b*) release from internal stores (Alnaes and Rahamimoff, 1975), or (*c*) direct injection (Miledi, 1973). Although the study reported here relates specifically to the voltage-dependent calcium conductance change in presynaptic terminals of the squid giant synapse, release of intracellular substances after membrane conductance changes to calcium is of general interest since it is a property common to many cell types (cf. Llinás and Heuser, 1977).

Traditionally, few preparations have allowed a direct study of the synaptic transmission process with electrophysiological access to both pre- and postsynaptic elements. However, recent interest in depolarization-release coupling has seen the development of various preparations, among them the lamprey giant synapse (Martin and Ringham, 1975), the giant Mauthner cell synapse (Auerbach and Bennett, 1969), the *Aplysia* central nervous system (Shapiro et al., 1980), the photoreceptor in the barnacle (Ross and Stuart, 1978) and certain central synapses in spiny lobster (Maynard and Walton, 1975; Graubard and Calvin, 1979), cockroach (Pearson and Fourtner, 1975), crab (Blight and Llinás, 1980) as well as other systems (cf. Pearson, 1979). Of these only the squid synapse and, to a lesser extent, the crab, lamprey and Mauthner lateral line system can routinely be impaled at the junctional site. While some differences between these junctions have been reported, there is no doubt that ultimately a general model for synaptic transmission may be developed.

Our experiments attempted to apply the voltage clamp technique (Cole, 1949) to measure

calcium conductance changes in the largest presynaptic terminal digit of the squid stellate ganglion. The aim was to describe in quantitative terms the relationship between transmembrane voltage and calcium permeability at this end fiber. The present paper is concerned with the voltage-dependent presynaptic calcium current while a second paper (Llinás et al., 1981) describes the relationships between calcium current and postsynaptic response (EPSP). Several preliminary communications have been made regarding part of this material (Llinás et al., 1976, 1979; Llinás, 1977).

METHODS

Preparation

Experiments were performed on small *Loligo pealii* at the Marine Biological Laboratory, Woods Hole, Mass. The mantle length of the specimens utilized ranged from 6 to 8 in. After decapitation, the stellate ganglion was removed from the mantle under running seawater and a 2-cm length of postsynaptic fiber (the most medial and largest of the tertiary axons) was tied off and isolated. The other postsynaptic axons were transected 2–3 mm from the borders of the ganglion. After isolation, the surface of the ganglion was denuded of its sheath of connective and muscular tissue, thus exposing the fin nerve (Young, 1939). This superficial nerve bundle was then removed to reach the synapse itself. Occasionally, further dissection was required at this point to remove connective tissue.

The isolated ganglion was held in a three-compartment chamber designed to allow rapid continuous superfusion of the preparation with a minimum of turbulence (Fig. 1 *A*). The pre- and postsynaptic fiber bundles were tied with thread and fixed in place by means of movable wedges. When necessary, "minuten pins" or cactus spines from *Notocactus haselbergii* were utilized to affix the ganglion to a thin layer of Sylgard covering the bottom of the chamber. The preparation was transilluminated and examined with a ×30 dissecting microscope.

In some preparations the entire presynaptic complex could be clearly seen. On these occasions the second-order giant fiber could be visualized entering the ganglion where it broadens to form a "palm" from which several branches emerge and end as a set of rather blunt terminal digits which contact the 8–10 giant tertiary axons. The synapse between the most distal digit and the most medial (and largest) of the third-order giant fibers was used in all our experiments and will be referred to in this paper as "the giant synapse." On the average, only 10% of the ganglia dissected could be utilized since the voltage clamp technique requires that several morphological criteria be met. First, the terminal digit must be located either directly above or to one side of the postfiber in such a way that its whole length may be clearly visualized. Presynaptic terminal digits having obvious constrictions or an irregular course were discarded since it was difficult to determine the exact position of the electrodes with respect to each other, this being an important variable. A typical synapse meeting the above criteria is shown in Fig. 1 *B*. It also became clear that the best synapses were those requiring minimal dissection; attempting to clear large amounts of connective tissue from the surface of this terminal often caused disruption of synaptic activity.

The presynaptic terminal digit in these squid is, on the average, 1.1–1.2 mm long with a diameter in the vicinity of 50 μm. The actual junction between the pre- and postterminals takes place between the smooth surface of the presynaptic digit and the spinelike processes of the postsynaptic fiber which partly embrace the presynaptic terminal (Young, 1973; Pumplin and Reese, 1978). For the most part, the area of contact is restricted to the distal two-thirds of the presynaptic digit. In particularly translucent junctions it is possible to observe, with a normal dissecting microscope, the rough edges which demarcate the contacts between the pre- and postsynaptic elements. Estimates of the extent of this synaptic contact were obtained in four junctions by postsynaptic injection of methyl blue dye and direct measurement of the length of the postsynaptic spiny surface. These measurements yielded an average length of ~700 μm, quite close to Young's (1973) estimate (650 μm). The exact location of microelectrode penetration is an

important variable in the voltage clamp techniques used and was noted for each experiment; electrode separation was determined microscopically.

Solutions

In most experiments the composition of the ionic media was 423 mM NaCl, 8.3 mM KCl, 10 mM $CaCl_2$, 50 mM $MgCl_2$. It was buffered to a pH of 7.2 with bicarbonate phosphate or Trizma buffer (Sigma Chemical Co., St. Louis, Mo.) and continuously oxygenated with a 99.5% O_2 and 0.5% CO_2 gas mixture or with 0.001% H_2O_2 (Llinás and Sugimori, 1980). In those experiments in which calcium concentration was varied, $[Ca^{2+}]_o$ ranged from 1 to 100 mM. Sets of voltage clamp results were obtained at $[Ca^{2+}]_o$ of 3, 5, 10, 20, 40, and 100 mM. Magnesium concentration was modified to keep the ionic strength constant except in the case of 100 mM Ca^{2+}, where the Mg was 20 mM. Sodium conductance (g_{Na}) was blocked by superfusions with tetrodotoxin (TTX) (Narahashi et al., 1964) at a concentration of 5×10^{-6} g/ml. Potassium conductance (g_K) was blocked by means of intracellular injection of tetraethylammonium (TEA) (Armstrong and Binstock, 1965) and by the addition of 5 mM 3- or 4-aminopyridine (3- or 4-AmP) (Pelhate and Pichon, 1974; Llinás et al., 1976; Yeh et al., 1976). These two types of g_K blockers were used simultaneously, as they operate within a slightly different voltage range. 3-AmP blockage is quite complete for levels up to 40–50 mV from rest. TEA blockage is most effective above 40 mV membrane depolarization. The slow calcium channel was blocked by adding manganese chloride at 10 mM (Hagiwara and Nakajima, 1966) or 1 mM cadmium chloride (Kostyuk and Krishtal, 1977; Llinás et al., 1979). All experiments were performed at 18°C. This temperature was kept constant by means of a Peltier effect feedback system.

General Electrophysiological Methods

After the procedures described above, a recording microelectrode was introduced into the postsynaptic fiber in the vicinity of the presynaptic digit. The location of choice was ~500 μm from the actual end of the presynaptic digit as this allowed maximum clearance for the two or three presynaptic microelectrodes. Initially, the whole presynaptic bundle was stimulated by means of a pair of stainless steel, teflon-coated wires positioned ~3–4 mm from the stellate ganglion (Fig. 1 *A*).

The microelectrodes which recorded potential (1 post- and 1 or 2 presynaptic) had an average DC resistance of 20 MΩ. Input capacity was neutralized by driven shield systems which extended close to the electrode tip (Fig. 1 *C*). We found this to be a crucial variable in attaining a fast voltage clamp (cf. Schwartz and House, 1970). The shielding was achieved by the use of a thin film of silver directly bonded to the glass by a special volatile resin carrier ("liquid organic silver" from Engelhard Electro Metallics, Newark, N.J.) which allowed the electrodes to be shielded to within 10–20 μm of the tip. The microelectrodes were isolated from the surrounding system by means of a water resistant compound (Humiseal) which produced an electrical insulation to ground of better than 10^{10} Ω. Often several coats of Humiseal were applied. The current injection electrode was prepared as described above, but the shield was grounded and the tip bevelled with a Brown instrument (Brown and Flaming, 1977) to a resistance of 3–5 MΩ.

In a given experiment all electrodes but one (the TEA pipette) were filled with 2.5 M potassium citrate and aged 1–2 wk. This aging increases the current-carrying capacity and reduces the Zeta potential of the electrodes (Agin, 1969). In most experiments, TEA was injected through one of the presynaptic recording electrodes which was filled with 1 M TEA bromide for this purpose. Since most commercially available TEA often produces toxic effects on nerve membrane, we synthesized our own using Armstrong's methanol purification procedure (C. Armstrong, personal communication).

Two methods were utilized for the TEA injection. In the first, outward current was injected through the TEA electrode and the current was returned through a second intracellular microelectrode. This method allowed presynaptic terminals to be filled with TEA quite readily since large current pulses (in the order of 1 μA) could be injected with minimal modification of the membrane potential. On other occasions, TEA was directly injected by means of a back-pressure air pulse (Llinás and Nicholson,

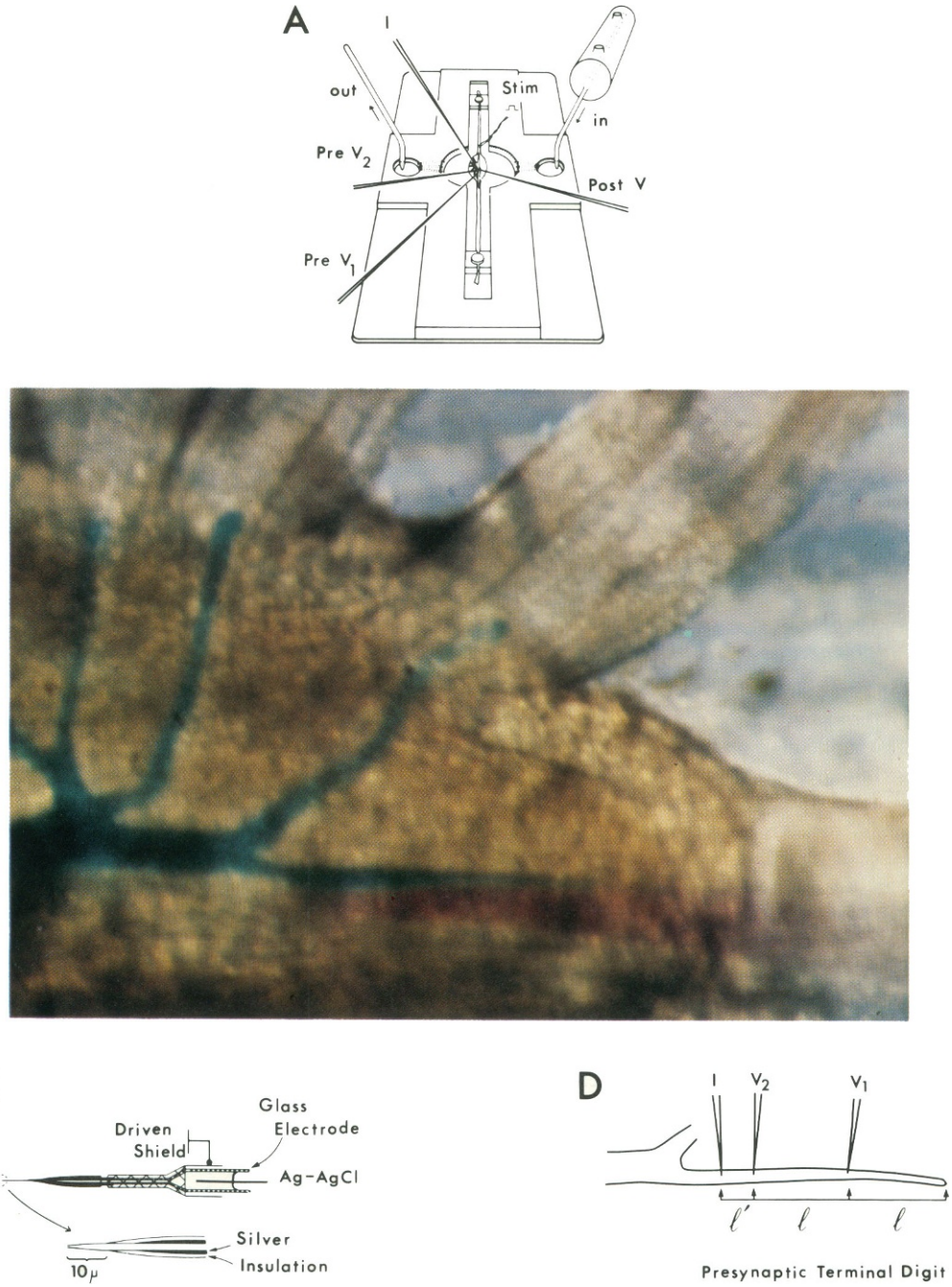

FIGURE 1 (*A*) Recording chamber. Artificial seawater is gravity fed into first reservoir (*in*) and removed after crossing center chamber from third reservoir via negative pressure (*out*). The two or three presynaptic micropipettes (*I*, Pre V_1 and Pre V_2) and the postsynaptic one (Post *V*) were spatially organized as indicated. The presynaptic nerve bundle was stimulated with a pair of stainless steel, teflon-coated wires (Stim). (*B*) Photograph of squid giant synapse showing the presynaptic fiber intracellularly stained with methyl blue and the postsynaptic intracellularly stained with arsenaso III (red). (*C*) Detail of microelectrode-driven shield. Silver metal was bonded to the glass electrode to within 10–20 μm of the tip and then insulated. The posterior part of the silver shield was not insulated to make contact with the rest of the shield by an elastic metallic cuff (cross-hatching). (*D*) Arrangement of presynaptic electrodes in the terminal (for further details, see text).

1975). The TEA injection was continued until a "complete" blockage of the voltage-dependent potassium conductance had ensued (see below).

Voltage Clamp Methodology

Two arrangements were utilized for the voltage clamp, involving either two or three microelectrodes. The electronics, electrode placement, and current measuring techniques used in both cases are described below.

ELECTRONIC EQUIPMENT The voltage clamp circuit utilized in these experiments is shown in Fig. 2 *A*. Presynaptic voltage was measured using an FET input operational amplifier (Analog Devices model 515, Analog Devices, Inc., Norwood, Mass.) Current was injected by means of a high voltage amplifier (Datel AM 303A, Datel, Inc., Holly Hill, Fla.). Total current was measured by means of a virtual ground circuit (Teledyne Philbrick 1439, Teledyne Philbrick, Dedham, Mass.). The indifferent electrode consisted of a large silver-silver chloride plate located across the bottom of the chamber. The speed of the voltage clamp, with the equipment described above, is illustrated in Fig. 2 *B*. This speed was attained in ~30% of the preparations where electrode placement and the morphology of the synapse were optimal. In most cases the time to plateau of the voltage microelectrode signal ranged from 50 to 150 μs.

For the three-electrode technique, the voltage difference (V_2 - V_1) between these voltage-sensing electrodes was obtained as shown in Fig. 2 using an AD521 differential amplifier. Recordings were displayed on an oscilloscope and photographed as well as put on digital tape for later analysis.

LEAKAGE CURRENT AND SERIES RESISTANCE In both the two- and three-electrode voltage clamps, leakage current, and most of the "make" and "break" transient artifacts were minimized using a Nicolet 1090A averager (Nicolet Instrument Corp., Madison, Wisc.) to subtract the current generated

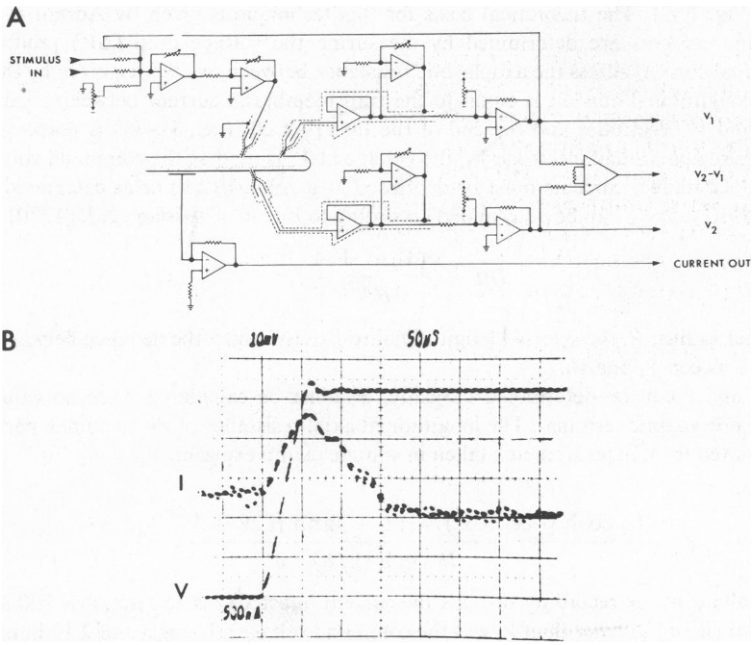

FIGURE 2 (*A*) Description of the voltage clamp circuit. The two-electrode voltage clamp consists of the upper portion of the circuit and involves V_1 and the current electrode shown to the left. The current was measured by a virtual ground (current out). The second technique measured the current as the difference between V_2 and V_1 (V_2–V_1 amplifier). For further details, see text. (*B*) Optimal speed for voltage clamp circuit showing three superimposed voltage steps (*V*) for 52 mV and the settling time for the current record (*I*).

by a hyperpolarizing pulse from that generated by a depolarizing pulse of the same amplitude. Errors due to series resistance, while small given the small amplitude of the calcium current, were corrected by means of a positive feedback system similar to that used by Hodgkin et al., (1952).

Current Measuring Techniques

MEASUREMENT OF TOTAL MEMBRANE CURRENT (Im_T) The method most frequently used to voltage clamp the preterminal utilized two microelectrodes, one for injecting current, which was placed ~700 μm from the blunt end of the presynaptic digit and a second for recording potential, which was located 350 μm from the end. In this case the total transmembrane ionic current activated by the voltage step (Im_T) was measured via a virtual ground system. Im_T was expressed either directly in nanoamps or as current density in $\mu A/cm^2$. The latter was calculated by dividing the recorded current by the surface area of the presynaptic terminal digit. Experiments where the presynaptic structure was impaled at multiple sites indicated that potential changes due to passing current at the normal current injection site are restricted by cable decrements mainly to the terminal digit itself. We make the working assumption that cable currents flowing from the terminal digit will behave as a linear leakage component and thus cancel out with the leakage current correction procedure described above. It is recognized, however, that errors may result from imperfect isopotentiality of the membrane area sensed by the two-microelectrode current measuring technique. The degree of inaccuracy of this technique was assessed by comparing the currents obtained by this method with those obtained using the three-electrode technique developed by Adrian et al., (1970). This comparison will be treated in detail later.

MEASUREMENT OF ΔV AND CALCULATION OF $Im_{\Delta V}$ This method, originally developed to voltage clamp single muscle fibers, utilized three electrodes (Adrian et al., 1970), one for current injection and two for voltage measurement. The current injecting electrode (I) is placed ~800 μm ($2\ell + \ell'$) and the V_2 and V_1 recording electrodes 700 (2ℓ) and 350 μm (ℓ), respectively, from the end of the terminal digits (Fig. 1 *D*). The theoretical basis for this technique is given by Adrian et al. (1970). Briefly, membrane currents are determined by measuring the voltage drop (ΔV) produced by the internal longitudinal current across the axoplasmic resistance between two points, given by the V_2 and V_1 electrodes. This longitudinal current is equal to the transmembrane current between a point midway between the V_1 and V_2 electrodes and the end of the fiber. As ΔV (i.e., V_2–V_1) is porportional to the current within the region around electrode V_1, the voltage at V_1 is used as the command voltage. Unlike the two-electrode technique, currents must be expressed as a voltage (ΔV) or as calculated membrane current density ($Im_{\Delta V}$). $Im_{\Delta V}$ can be determined according to Eq. 10 of Adrian et al. (1970):

$$Im = \frac{a(V_2 - V_1)}{3R_i\ell^2}, \tag{1}$$

where a is the fiber radius, R_i the internal longitudinal resistivity, and ℓ the distance between end of the fiber and V_1 and between V_1 and V_2.

Values for a and ℓ can be determined optically, R_i must be calculated since no value has been published for the presynaptic terminal. The longitudinal axial resistance of the terminal, per unit length (r_i), can be calculated from measurements taken in voltage clamp experiments using Eq. 3 of Chandler et al., (1976):

$$r_i = \frac{V_1 \cosh\left[(2\ell + \ell')/\lambda\right](1 + \tanh\left[(2\ell + \ell')/\lambda\right])}{I\lambda \cosh\left(\ell/\lambda\right)}, \tag{2}$$

where V_1 is the voltage at the recording site, I is the current injected, ℓ is 350 μm, ℓ' is 100 μm, and λ is the length constant (here V_2 rather than V_1 was the command voltage). Using a λ of 2.12 mm (calculated with Eq. 2 of Chandler et al., 1976) values of 3.44 and 4.04 MΩ/cm are obtained for r_i (giving internal resistivities of 67.5 and 79.3 Ωcm). R_i can also be determined from current clamp experiments such as shown in Fig. 3. Here values of 2.65 and 2.75 mm were obtained for λ. Values for r_i were then calculated from the definition of the space constant ($\lambda = \sqrt{r_m/r_i}$ where r_m is the specific membrane resistance) and membrane resistances (R_m) of 1.42 and 1.64 kΩcm^2 were calculated from the input resistances. Values for r_i of 1.28 and 1.38 MΩ/cm give internal resistivities (R_i) of 25.12 and 27.08 Ωcm, respectively.

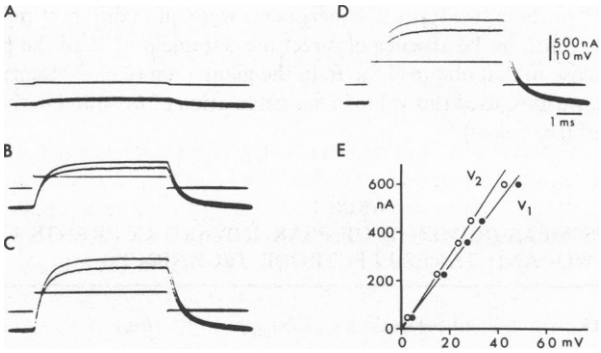

FIGURE 3 Measurement of length constant (λ) with microelectrode placement as shown in Fig. 1 *D*: ℓ 350 μm, ℓ 100 μm. (*A–D*) Recordings used to measure λ. (*E*) Plot of current voltage relationship for V_1 and V_2 electrodes.

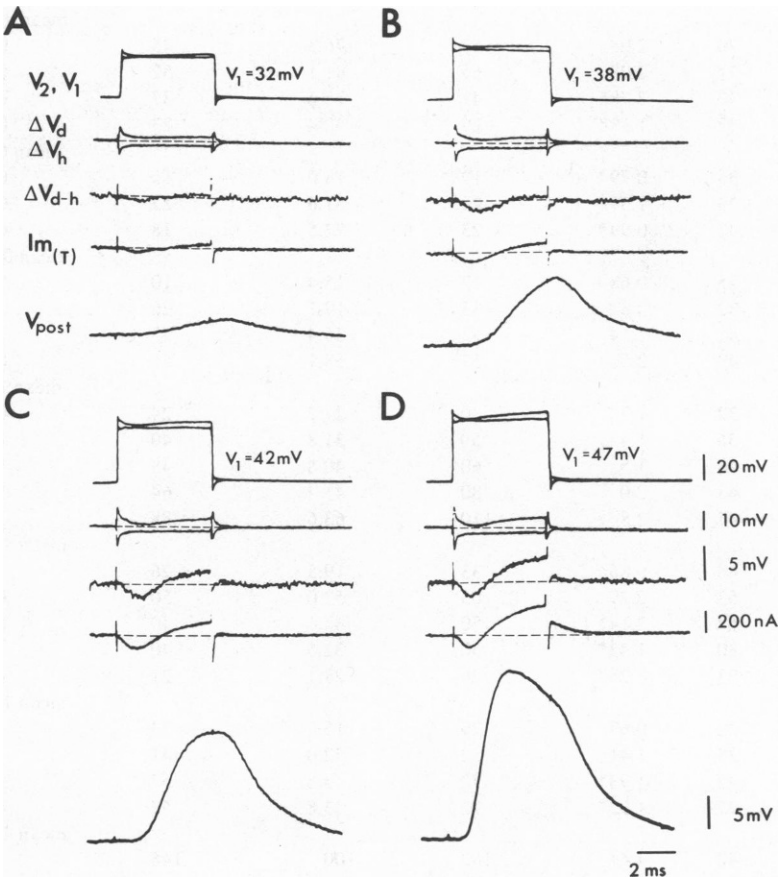

FIGURE 4 Measurement of current as ΔV at four levels of voltage clamp. (*A–D*) First trace, voltages recorded by V_1 and V_2 electrodes. Second trace, V_2–V_1 for depolarizing (ΔV_d) and hyperpolarizing (ΔV_h) pulses. Third trace, difference between ΔV_d and ΔV_h giving ΔV. Fourth trace, "total current" ($Im_{(T)}$ measured via virtual ground after leakage subtraction. Last trace, postsynaptic response. G_{Na} has been blocked with TTX, and G_K has been partially blocked with TEA/3-AmP. Note that ΔV and $Im_{(T)}$ have a similar time course. Due to incomplete g_K blockage, amplitude of inward current records is reduced by outward current; however, increasing postsynaptic potential indicates increasing calcium currents. $[Ca^{2+}]_o$ = 10 mM.

The values for R_i obtained in these two types of experiments were quite different reflecting the limit of the measuring techniques. Thus, in the absence of direct measurement of R_i in the preterminal, and since the latter values were close to that obtained for R_i in the giant axon (e.g., 30 Ωcm), determined by direct methods (Cole, 1968), we have used this value in our calculation of $Im_{\Delta V}$ and in the formulation of our models of the preterminal (see below).

TABLE I
SIMULTANEOUS MEASUREMENTS OF PEAK INWARD CURRENTS USING TWO- AND THREE-ELECTRODE TECHNIQUES

Synapse No.	V_t	ΔV	"Total current"	$Im_{(\Delta V)}$	$Im_{(T)}$	$\frac{Im_T}{Im_{\Delta V}}$
	(mV)	*(mV)*	*(nA)*	*(μA/cm²)*	*(μA/cm²)*	
S 788	34	0.4	18	9.08	14	1.54
	36	0.99	38	22.5	30	1.33
	42	1.59	66	36.1	53	1.47
	55	2.68	132	61.0	105	1.72
						mean 1.52 ± 0.16
S 352	20	2.08	57	76.2	45	0.59
	34	2.98	65	81.1	52	0.62
	40	2.78*	47	75.6	37	0.49
	52	1.19*	29	32.4	23	0.71
						mean 0.6 ± 0.09
S 354	35	0.79	19	18.0	15	0.83
	39	1.39	28	31.6	22	0.70
	42	0.99*	23	22.5	18	0.80
						mean 0.78 ± 0.07
S253	25	0.68	12	15.4	10	0.65
	32	0.82	33	19.1	26	1.36
	41	1.54	54	35.4	43	1.21
	49	2.56	57	58.1	45	0.78
						mean 1.0 ± 0.34
S 221	32	1.2	30	27.2	24	0.88
	36	1.4	50	31.8	40	1.26
	40	1.5	60	40.8	48	1.18
	43	2.0	80	45.4	64	1.40
	47	2.8	110	63.6	88	1.38
						mean 1.22 ± 0.21
S 254	40	0.86	33	19.5	26	1.33
	53	2.29	63	52.0	50	0.96
	67	2.14*	50	48.6	40	0.82
	80	1.43*	50	32.5	40	1.23
	93	1.28*	26	29.1	21	0.72
						mean 1.02 ± 0.26
S 111	32	0.67	29	15.2	23	1.51
	38	1.41	52	32.0	41	1.28
	42	1.93*	72	43.8	57	1.30
	47	1.93*	72	43.8	57	1.30
						mean 1.35 ± 0.11
S 725	40	4.41	183	100	146	1.46
	50	13.6	450	309	358	1.16
	80	5.42	250	123	199	1.62
						mean 1.41 ± 0.23

*Significant outward current. $Im_{(\Delta V)}$ calculated using Equation 1 with R_i = 30 Ωcm, a = 25 μm, ℓ = 350 μm. $Im_{(T)}$ calculated using an effective membrane area ($2\pi al$) of 12.56 × 10^{-4} cm² with a = 25 μm and ℓ = 800 μm.

Examples of recordings obtained using the three-electrode voltage clamp technique are shown in Fig. 4. Although not typical, since there is a significant outward current, this particular set of records was chosen because they illustrate most aspects of the use of this technique in the present preparation.

Fig. 4 illustrates the measurement of ΔV. The first trace of each set of records shows the voltages recorded at V_1 and V_2 (see Fig. 1 *D*). The next trace shows ΔV for depolarizing and hyperpolarizing clamp pulses and the third trace gives the difference between these measurements. For comparison, the fourth trace is the total transmembrane current. Finally, the postsynaptic response is shown. As can be seen in Fig. 4 *A–D*, the inward current increases with clamp voltage amplitude. However, in this case, a late outward current is also apparent, due to incomplete blockage of the potassium conductance. This outward current increases with depolarizing clamp pulse amplitude (*C* and *D*) and cuts short the inward current which does not seem to increase between *C* and *D*. However, the increased amplitude of the EPSP indicates a sizeable increase in calcium current. Thus, in this case neither ΔV nor Im reflect accurate calcium current amplitudes for the high voltages.

The experiment, however, can serve to set some limits on the accuracy of the method as applied to this preparation. More importantly perhaps, it does provide evidence for the degree of longitudinal anisopotentiality along the preterminal digit, even in the presence of a significant outward current (maximum ΔV for the potassium current was 3.52 mV). Table I gives values for ΔV, $Im_{\Delta V}$, and Im_T measured with three electrodes in a set of eight experiments.

Comparison of Two- and Three-Electrode Current Measurements

Comparisons of Im_T and $Im_{\Delta V}$ measurements indicate that the time courses of the inward currents are quite similar regardless of the method utilized (Figs. 4 and 5). Of the two variables—time course and amplitude—the time course can be compared directly and is the more important since it indicates that the "total current" measured is largely restricted to the terminal digit under study. Simultaneous recordings of "total current" and ΔV are shown in Fig. 5. Here, to facilitate comparison of the time course of the two current measurements, the gain of the ΔV trace was chosen such as to match the displayed amplitude of Im_T. Superimposition of the two traces ΔV and $Im_{\Delta V}$, is shown in the bottom line in each set of records and demonstrates a close correspondence between the two recordings for depolarizations of 42 and 55 mV; at lower levels of depolarization the onset of the Im_T trace is slightly slower than that for ΔV, while the time course for the tail currents is quite similar. In general, the time course of the two types of current measurement correspond well, indicating that the "total current" does reflect the inward calcium current in the clamped terminal digit.

Comparing the amplitude for these two types of current measure is, on the other hand, not as straightforward since, as described above, current density must be calculated from ΔV with Eq. 1. This equation is derived for a uniform cylinder (which the presynaptic terminal only approximates) and includes a term for the internal longitudinal resistance (r_i) which itself must be determined independent-

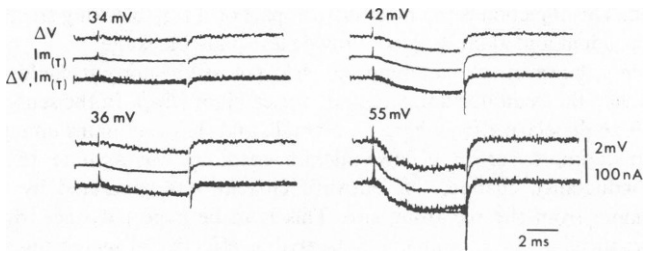

FIGURE 5 Comparison of total (Im_T) and V_2–V_1 (ΔV) currents at four voltage clamp levels after blockage of g_{Na} and g_K. Records were obtained by subtracting currents generated by symmetrical depolarizing and hyperpolarizing voltage clamp pulses of the same ampltiude. In each set of records: top trace, current using a two-electrode voltage clamp; middle trace, current measured using three-electrode technique; bottom trace, superimposition of two- and three-electrode recordings. Note that the current follows a similar time course with both recording techniques. $[Ca^{2+}]_o$ = 10 mM.

ly. The values obtained for $Im_{\Delta V}$ depend additionally on electrode placement. Nevertheless, to determine an estimate of the degree of difference obtained for I_{Ca} by the two techniques, current density was calculated from measurements of total current and ΔV.

Table I (last column) gives a direct comparison of these two current measurements for eight different experiments, over the most sensitive range (20–50 mV clamp pulses from rest). The results indicate similar values of Im with both techniques. Divergences of values do occur at higher voltage steps as the outward potassium current tends to be more prominent in Im_T since in this case total transmembrane current includes I_K from the nonsynaptic portion of the terminal. Occasionally, $Im_{\Delta V}$ was slightly larger than Im_T. This discrepancy falls within the expected range of error of the technique (Adrian et al., 1970; Kass et al., 1979). We conclude, therefore, that within the limits of accuracy of the techniques utilized, Im_T measured as described in this paper represents quite closely the actual time course and amplitude of the calcium current flowing during the voltage clamp step at the terminal under study.

Degree of Voltage Clamp Control

The question of voltage control is quite important as sudden jumps in inward current may be observed during the voltage clamp pulse. These jumps generally occur at higher voltages and may be seen as an all-or-none response at voltage levels close to maximum inward current and especially during the tail current. On some occasions, rather than the above all-or-none response, an obvious deviation of the tail current from an exponential decay, which varies from one trial to another, may be present. In such instances, a secondary component for the postsynaptic potential is often observed during the "on" or "off" EPSP, implying that voltage control has been lost at the terminal under clamp. Occasionally, during large depolarizations, such inward currents do not generate postsynaptic potentials, indicating that they are produced by the activation of other digits in this terminal. This is an important source of error as it can obscure the smooth onset of the current, making it appear more square if it happens in the initial part of the clamp step, or can distort the tail current.

Potassium Conductance in the Presynaptic Terminal

Two principal types of potassium conductance have been observed at the presynaptic digit. The first is a voltage-dependent potassium conductance change as described by Hodgkin and Huxley (1952 *a* and *b*). This current can be easily observed with voltage clamp applied before the complete blockage with TTX and TEA/3-AmP. An example of such an experiment is shown in Fig. 6. The level of depolarization could only be increased to 38 mV, since beyond that point a presynaptic spike was generated due to loss of clamp control. Note, however, that with partially blocked g_{Na} and g_K, postsynaptic potentials can be clearly seen even when, at the higher voltage steps, a predominantly outward current is seen at the preterminal. This voltage-dependent potassium current can be blocked quite completely by the TEA/3-AmP combination such that no outward currents are seen when the TEA injection has been successfully performed. This injection is the more critical part of the g_K blocking since the 3-AmP effect is time and voltage-dependent and alone does not provide adequate blockage.

In many experiments, however, a remaining outward potassium current could be seen when the depolarization approached the "equilibrium potential" for calcium (E_{Ca}). In the sense that this outward current was found at high depolarization where I_{Ca} is small, and that it remains intact after blockage of calcium current with cadmium or in a low calcium medium, we assume that, rather than a calcium-dependent conductance change, this outward current was generated by voltage-dependent potassium current remote from the recording site. This is to be expected since, due to intracellular dilution, the TEA introduced at the terminal is probably less effective at increasing distances from the site of injection.

The second type of potassium current was related to calcium entry (Meech, 1978). In this case, an absence or decrease of inward calcium current was accompanied by a decrease of late outward current (7–10 ms after onset of the pulse). Because this component was quite variable and inconstant, it will not be considered further. Also, given that in the present study the pulse duration was generally too short to activate the calcium-dependent g_K, such data are not included here.

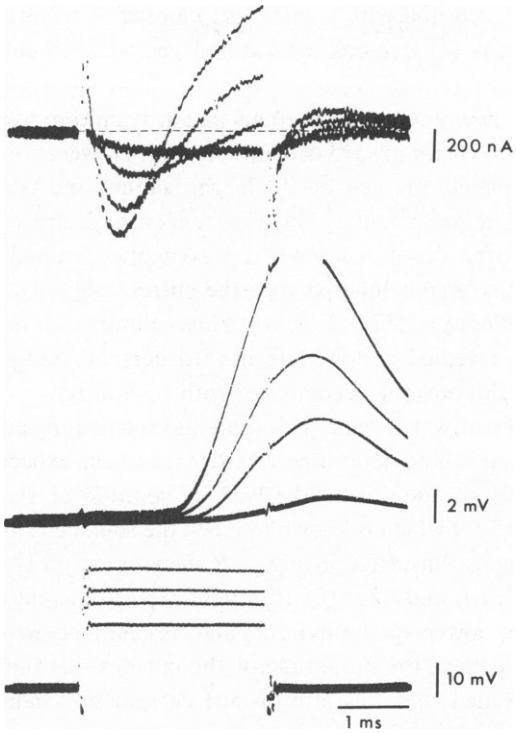

FIGURE 6 Two-electrode voltage clamp showing sodium and potassium currents in a presynaptic terminal. Top traces, current; middle, postsynaptic response; bottom, voltage clamp pulses. At voltages beyond those illustrated, the clamp circuit lost control and the presynaptic terminal generated a sodium action potential although g_{Na} and g_K were partly blocked by TTX and 3-AmP, respectively. $[Ca^{2+}]_o$ = 10 mM.

RESULTS

The present set of data was obtained from ~100 successful voltage clamp experiments. Twelve of these utilized the three-electrode voltage clamp technique and were carried out to check the validity of the two-electrode voltage clamp. The experiments selected for the present measurements and illustrations (see Table III) fulfilled the following criteria: (*a*) Clamp pulses of at least 80 mV were achieved (from a holding potential of -70 mV). (*b*) Currents were

TABLE II
TIME CONSTANTS OF TAIL CURRENTS

Synapse No.	μs	SD	*n*
S 63	674	±68	9
S 823	665	±121	10
S 76	651	±101	14
S 818	441	±102	9
S 75	426	±59	9
S 727	418	±65	17

taken at enough clamp levels and with a sufficient number of trials at each level to reliably establish I–V relationships. (*c*) Records showed no large outward currents or loss of voltage clamp control.

As stated above, it is now generally accepted that transmitter release is triggered by an increase in $[Ca^{2+}]_i$ usually via an inward calcium current. However, during normal transmission this current is completely masked by the larger sodium and potassium currents which generate the presynaptic action potential. Such currents are illustrated in Fig. 7 *A* where the total membrane current after depolarization of a presynaptic terminal with partial g_{Na} and g_K blockage (Fig. 7 *A*, *a*) has been compared with the current obtained, with the same voltage step, after "complete" blockage (Fig. 7 *A*, *b*). Thus, elimination of the sodium (I_{Na}) and potassium (I_K) currents revealed a slow, late inward current. Note the difference in time course and amplitude of this current as compared with I_{Na} and I_K.

Since this inward current was a regular finding and seemed to relate directly to synaptic transmission, our first step was to determine whether it was, as expected, carried by calcium ions. This was tested by the addition to the bathing solution of 1 mM cadmium chloride (Kostyuk and Krishtal, 1977) which is known to block the so-called slow calcium channel. An example of such blockage is illustrated in Fig. 7 *B* showing currents measured for the same voltage clamp step before (*a*) and after (*b*) 10 min of exposure to cadmium chloride. Similar results were obtained by lowering the extracellular calcium below 0.5 mM or by adding manganese chloride. Further, the amplitude of the current was found to be dependent on $[Ca^{2+}]_o$. Thus, we concluded that this late inward current was indeed carried by calcium ions.

Four general properties of this current were studied: first, its time course and amplitude at different levels of presynaptic clamp depolarization; second, the properties of the "off" or tail currents; third, the instantaneous current; and fourth, the relation between $[Ca^{2+}]_o$ and steady-state calcium currents, I_{Ca}^{∞}.

Time Course and Amplitude of Calcium Currents

Inward currents typical of those seen when the presynaptic terminal is clamped after TTX and TEA/3-AmP treatment at the normal $[Ca^{2+}]_o$ (10 mM) are shown for two different

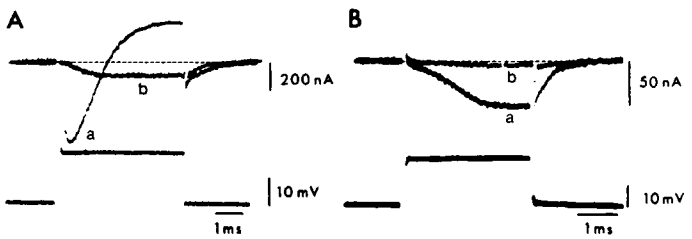

FIGURE 7 Comparison of time course of sodium and potassium currents with the calcium current and blockage of the calcium current by cadmium chloride. (*A*) Time courses for sodium and potassium currents after partial blockage of sodium by 10^{-9} g/ml TTX and of potassium by 0.5 mM 3-AmP (*a*). The next record (*b*) was obtained in the same synapse and at the same level of presynaptic depolarization after 5×10^{-6} g/ml TTX and 5×10^{-3} 3-AmP and intracellular injection of TEA. Note time course and amplitude of inward current. (*B*) In another synapse, inward current after blockage of g_{Na} and g_K (*a*) and after addition of 1 mM cadmium chloride to the bath (*b*). Two-electrode voltage clamp technique. *A*, *b*, and *B* currents subtracted. $[Ca^{2+}]_o$ = 10 mM.

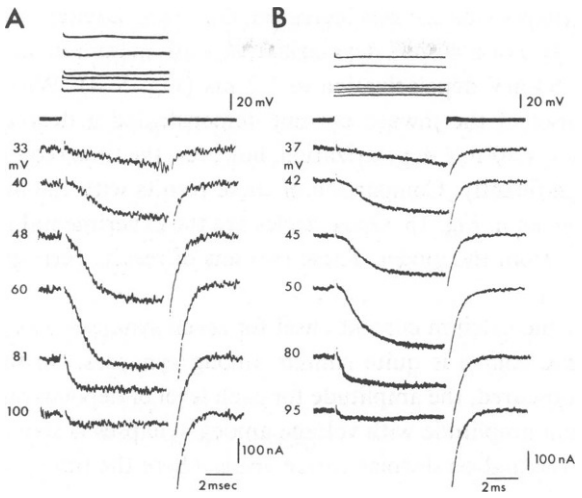

FIGURE 8 Calcium current. (*A* and *B*) Currents recorded at different levels of presynaptic depolarization in two synapses. Note the S-shape of the current onset and the fast tail current. Two-electrode clamp technique; currents subtracted. $[Ca^{2+}]_o$ = 10 mM.

experiments in Fig. 8 *A* and *B*. These two sets of results were selected because the duration of the current pulses were quite similar, and the potassium blockage almost complete. As in all other experiments, the preterminal was clamped to different levels from a holding potential of -70 mV. In both cases illustrated, the inward calcium current was characterized by a slow onset and a plateau value that could be maintained unmodified for protracted periods. In short, then, these currents (Fig. 8 *A* and *B*) are characterized by a sigmoidal onset, a voltage-dependent rate of rise and amplitude, and the absence of inactivation, at least for the duration of the voltage steps (in some experiments as long as 100 ms).

TIME COURSE A detailed investigation of these currents demonstrated that as the

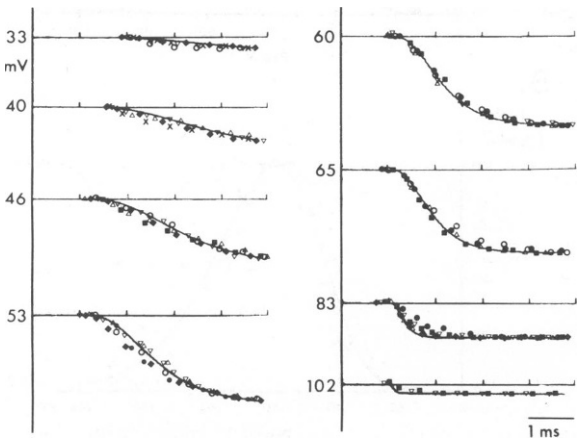

FIGURE 9 Time course of the calcium current. Solid lines represent solution to Eq. 15 for voltages given at the left. Symbols are experimental results from seven synapses. Currents were normalized by setting the maximum current for each voltage to 100%. Two-electrode voltage clamp technique; currents subtracted. $[Ca^{2+}]_o$ = 10 mM.

amplitude of the presynaptic voltage was increased, both their latency and rise time decreased (Figs. 8 *A* and *B*, and 9). For a 40-mV depolarization, half maximum amplitude was reached in 2.13 ms, and for a 60-mV depolarization in 1.2 ms (Fig. 8 *A*). With increasing levels of depolarization, the onset of the inward current demonstrated a decrease in latency and a faster rate of rise. Beyond 80-mV depolarization, however, the time required to reach one-half I_{Ca}^{∞} did not change significantly. Comparison of these results with the numerical solution for Eq. 15 (see below) is given in Fig. 16. Open circles are the experimental results and solid lines the numerical solution from the model. These two sets of results correspond well and will be discussed below.

The time course of the calcium current onset for seven synapses was plotted in Fig. 9 and indicates that this time course is quite similar among synapses. So that the shape of the current traces not be obscured, the amplitude for each level of depolarization was normalized. The variation in current amplitude with voltage among synapses is shown in Fig. 10 *B*. Most variation was seen at the highest depolarization levels where the time course of current onset was sometimes slower than expected.

AMPLITUDE This parameter, the value of the peak inward current, was probably the most variable measurement among experiments (Table III). This is not surprising given the differences in preterminal morphology. The relationship between the amplitude of the

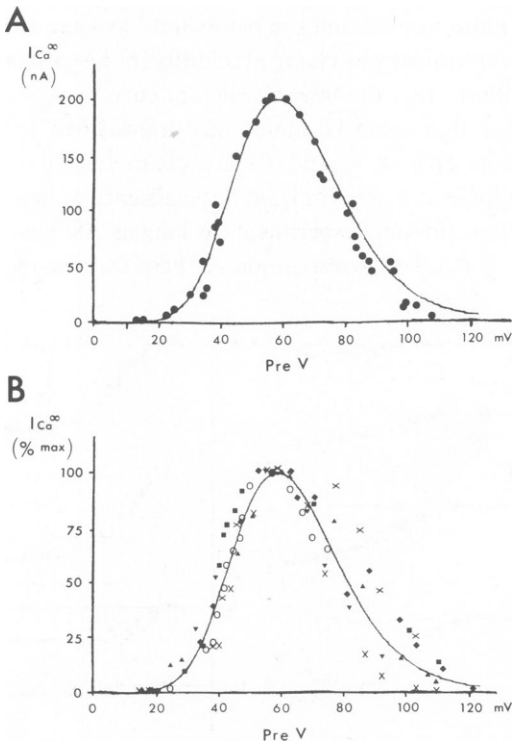

FIGURE 10 (*A*) Plot of peak calcium current (I_{Ca}^{∞}) against a presynaptic voltage. Peak amplitude occurs at ~60 mV depolarization. Solid line indicates numerical solution for I_{Ca}^{∞} of Eq. 17 of our model. (*B*) Voltage dependence of I_{Ca}^{∞} for eight synapses. I_{Ca} is plotted as a percentage of maximum current. $[Ca^{2+}]_o$ = 10 mM.

presynaptic depolarization and the amplitude of the inward steady-state calcium current (I^{∞}_{Ca}) was plotted in Fig. 10 *A* for one synapse. As seen in that figure, I^{∞}_{Ca} followed a bell-shaped curve with a rather rapid rise. (Between 25 and 35 mV the current increased exponentially; an *e*-fold increase occurred in 5 mV.) Due to the noise level of our current measurements, at 10 mM $[Ca^{2+}]_o$ an inward current was first clearly discernible at ~20 mV depolarization. However, we have shown that synaptic release in this junction is a continuous function of membrane potential (cf. Llinás, 1979).

With increasing levels of depolarization, as shown in Figs. 8 and 9 and plotted in Fig. 10, I^{∞}_{Ca} increased to a maximum near 60 mV depolarization. From this level onward, the magnitude of the current diminished such that at 115 mV depolarization only a very small inward current could be observed during the voltage step and reached a near zero level ~130–140 mV from resting. It must be noted that in none of our experiments was there any sign of an outward calcium current. This is not surprising since the $[Ca^{2+}]_i$ is on the order of 10^{-7}–10^{-8} M (Blaustein, 1974; Di Polo et al., 1976). In fact, at high depolarizations, the

TABLE III
PRESYNAPTIC CURRENTS AT VARIOUS $[Ca^{2+}]_o$

Synapse No.	$[Ca^{2+}]_o$	Onset	Max. peak I^{∞}_{ca}	"E_{Ca}"
	(mM)	*(mV)*	*(nA)*	*(mV)*
S 714	3	23	168	—
S 818	3	—	175	—
S 819	3	25	150	—
S 823	3	21	65	—
S 119	10	—	290	130
S 139	10	23	190	134
S 259	10	25	294	136
S 528	11	20	—	—
S 714-0	10	17	210	117
S 714-1	10	21	110	120
S 714-2	10	24	140	—
S 714-3	10	23	320	—
S 717-1	10	24	216	—
S 753	10	16	160	140
S 754-1	10	20	133	—
S 754-2	10	20	297	—
S 754-3	10	22	327	112
S 754-4	10	24	324	120
S 818-1	10	24	242	—
S 818-2	10	27	370	—
S 874	10	24	250	111
S 875	10	25	289	—
S 69	20	24	—	—
S 714	20	26	350	140
S 825	20	—	80	—
S 619	40	21	—	—
S 818	40	29	760	125
S 819	40	19	570	—
S 714	100	23	840	—

calcium current decreased asymptotically, making the estimation of a reversal potential, by extrapolation, very difficult. The variation seen in the voltage dependence of I_{Ca}^{∞} can be seen in Fig. 10 *B* where values obtained from eight preparations are plotted. Since the absolute value for the maximum current varied among synapses (see Table III), probably due to differences in digit size, currents were normalized, taking the maximum current in each synapse as 100%. As is evident from plot *B* in Fig. 10, the relation between prevoltage and I_{Ca}^{∞} is quite similar among synapses. There is, however, a variation in the relative amplitude during the falling phase of the plot, probably due to the degree of isopotentiality obtained in different synapses at high membrane polarizations. The solid lines in Fig. 10 are the numerical solution for Eq. 17 which describes the voltage dependence of I_{Ca}^{∞}.

Calculation of Calcium Conductance

The usual procedure, first introduced by Hodgkin and Huxley (1952 *a*), of expressing currents in terms of conductances cannot be directly followed in this case. In addition to the difficulty of determining E_{Ca}, conductance as classically defined for an ionic species m, as $g_m = I_m/(V-E_m)$, is not directly applicable here, for this definition is useful only as long as the conductance per open channel is ohmic, i.e., independent of the membrane potential. From analysis of the instantaneous currents (Fig. 12) we have determined that this is not the case for the calcium conductance at this terminal. However, as will be seen later, it is possible to calculate a value for calcium conductance if the nonlinear voltage dependence for the driving force is taken into account (see Eqs. 19 and 20).

Tail Current

Historically, the study of tail currents has been one of the most valuable ways to determine the kinetics of voltage-dependent ionic conductances, as well as to check the validity of the independence principle (Hodgkin and Huxley, 1952 *a*). One important parameter which can be established by such measurement is the time dependence for the closing of the ionic conductance channels. An example of a typical tail current is shown in Fig. 11 *A* and *B*. Here the terminal was clamped close to the null level for I_{Ca} where the steady-state current was zero. The time constant for this current was 633 μs. In these experiments the clamp pulse was returned to the initial holding potential (-70 mV). Since under such conditions, the time constant for the tail current does not vary with prepulse voltage, mean values were determined for five synapses from the semilog plots used to determine their amplitudes (Table II).

The amplitude of the tail current was determined as described above for several different levels of depolarization in five synapses (Fig. 11 *C* and *D*). Fig. 11 *C* shows the voltage dependence of both the steady-state and tail currents in a single synapse. The tail currents increased sharply for increasing levels of depolarization up to ~80 mV, at which point they began to level off. The same pattern can be seen in Fig. 11 *D* where measurements from the four other synapses were plotted; here the currents have been normalized with respect to the maximum steady-state current which was set at 100%. Solid lines in Fig. 11 *C* and *D* are numerical solutions for Eq. 15.

In short, the above results indicate that the decay of the tail calcium current in the presynaptic fiber may be described as close to a single exponential, the time course of this current being a fraction of that observed for the "on" currents at low depolarizations.

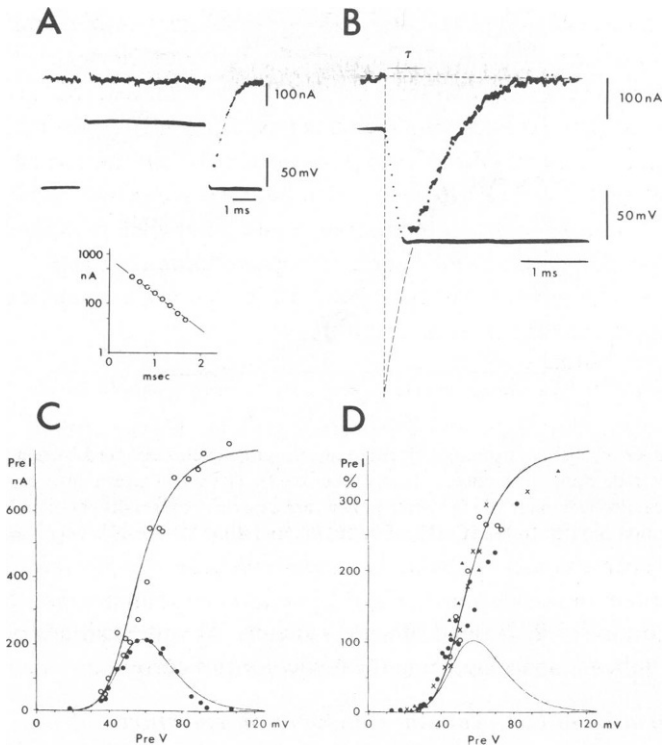

FIGURE 11 Tail currents. (*A*) Current obtained at clamp level near E_{Ca}. Note that there is no "on" current but a large "off" tail current. Shown below is a semilogarithmic plot of the current shown in *B*, indicating a close to single exponential decay for the tail current. (*B*) Tail current as shown in *A*, at higher gain and sweep speed. Dotted line gives extrapolation to "break" in voltage pulse (τ = 633 μs). (*C*) Amplitude of "on" current (filled circles) and tail current (open circles), and its comparison with numerical solutions for Eq. 17. (*D*) Tail currents obtained from four experiments with I_{Ca} expressed in percentage of peak "on" amplitude. *A* and *B*, $[Ca^{2+}]_o$ = 40 mM; *C* and *D*, $[Ca^{2+}]_o$ = 10 mM.

Instantaneous Currents

A second parameter which can be established from tail current measurements is the "instantaneous" current-voltage relationship (Hodgkin and Huxley, 1952 *b*). This relationship indicates whether the channel is ohmic and may also be used to test the independence principle. It has also been employed to estimate the equilibrium potential and, in addition, provides a good estimate of the degree of control of the voltage clamp itself. Three sample records obtained from a double pulse experiment at $[Ca^{2+}]_o$ of 10 mM are shown at the top of Fig. 12. In this synapse the initial voltage (V_I) was 60 mV and the second voltage (V_{II}) varied from 0 to 60 mV (dots in plot). The duration of each pulse was 4 ms. As in the previous case, the present tail current amplitudes were determined by extrapolation to the end of the pulse as shown in Fig. 11 *B*. A plot of the instantaneous current as a function of V_{II} is illustrated in Fig. 12 for five synapses and indicates that the instantaneous current in this terminal is not a linear function of voltage. The solid line is the calculated value for the instantaneous current as determined for 10 mM external calcium by solving Eq. 16 (see below). The insert gives the

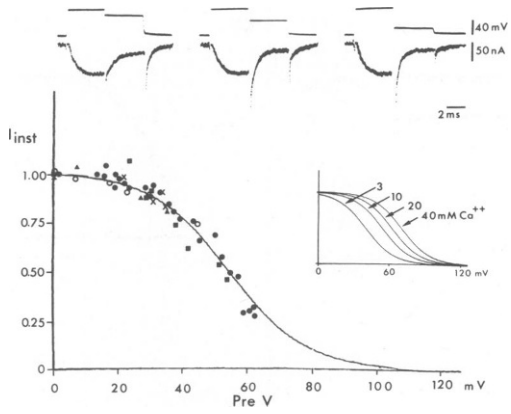

FIGURE 12 Upper records are examples of instantaneous tail currents obtained by double pulse voltage clamps (two-electrode clamp technique, currents subtracted). The graph gives numerical solutions of Eq. 16, with the calculated values for 10 mM $[Ca^{2+}]_o$. Dots are experimental results obtained for five synapses. Inset shows solution for Eq. 16 for $[Ca^{2+}]_o$ of 3, 10, 20, and 40 mM. Pre V is expressed relative to the holding potential.

solution to Eq. 16 for 3, 10, 20, and 40 mM calcium. The implications of this finding are discussed below in the section concerning the model for this current.

Relation of I_{Ca} to Extracellular Calcium Concentration

The effect of changes in $[Ca^{2+}]_o$ on transmitter release is one of the most thoroughly studied topics regarding the mechanism for synaptic transmission and yet one yielding the most variable results. (For studies in squid synapse, see Takeuchi and Takeuchi, 1962; Kusano et al., 1967; Katz and Miledi, 1969 *a* and *b*, 1970; Kusano, 1970; Lester, 1970). A full treatment of this subject will not be attempted at this time; we will present only some aspects of this complex problem. An important point to determine is to what extent $[Ca^{2+}]_o$ modifies I_{Ca}. As illustrated in Fig. 13 for 3 and 40 mM $[Ca^{2+}]_o$ and in Fig. 8 for 10 mM $[Ca^{2+}]_o$, the time course of the calcium current is very similar for these three calcium concentrations. The time course for the current then is dependent on the transmembrane voltage rather than the $[Ca^{2+}]_o$. However, as shown in Fig. 14 and Table III, the amplitude of I_{Ca}^{∞} is clearly related to $[Ca^{2+}]_o$. The steady-state calcium current reached at different levels of depolarization is plotted for three external calcium concentrations in Fig. 14. Several points are to be noted: (*a*) The rate of increase in I_{Ca} with voltage is dependent on $[Ca^{2+}]_o$. (*b*) The maximum I_{Ca} moves to the right with increased $[Ca^{2+}]_o$. (*c*) According to Eq. 17 the relationship between $[Ca^{2+}]_o$ and steady-state I_{Ca} measured at 60 mV is not linear and begins to saturate above 10 mM. This, however, has not been adequately tested experimentally as it requires a large set of data obtained at several levels of $[Ca^{2+}]_o$.

The results obtained from the numerical solutions of Eq. 17 for 3, 10, and 40 mM $[Ca^{2+}]_o$ are given as continuous lines in Fig. 14. Clearly there is good agreement between the experimental results and the numerical solution of the mathematical model. In addition, since the resolution of our clamp did not allow us to measure very small currents, the dependence of I_{Ca} "threshold" on $[Ca^{2+}]_o$ could not be determined. However, the model predicts that the "threshold" voltage for I_{Ca} is independent of $[Ca^{2+}]_o$.

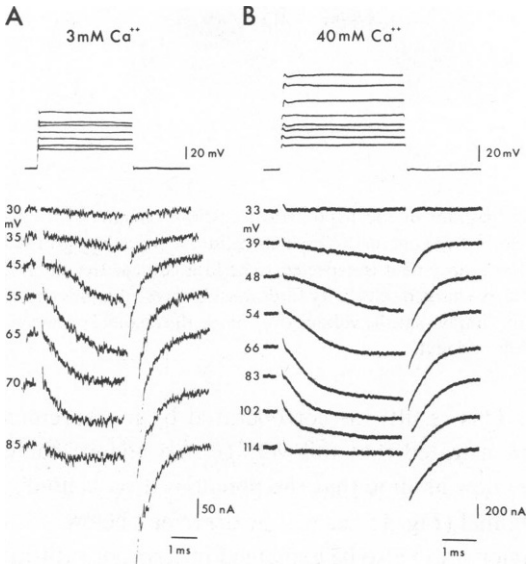

FIGURE 13 Sets of calcium currents recorded in 3 and 40 mM external calcium. The amplitude of these currents is significantly dependent on $[Ca^{2+}]_o$ (note calibrations) while their time courses are similar. Note that the tail currents in 3 mM calcium are large with respect to the steady-state currents while this is not the case for 40 mM calcium. Two-electrode voltage clamp technique; currents subtracted.

Kinetic Model for Inward Calcium Current

The present model represents a refinement of that presented previously (Llinás et al., 1976). The main difference concerns the deletion of the assumption of a constant electric field along the ionic channel. This modification came from our studies of the voltage dependence of the

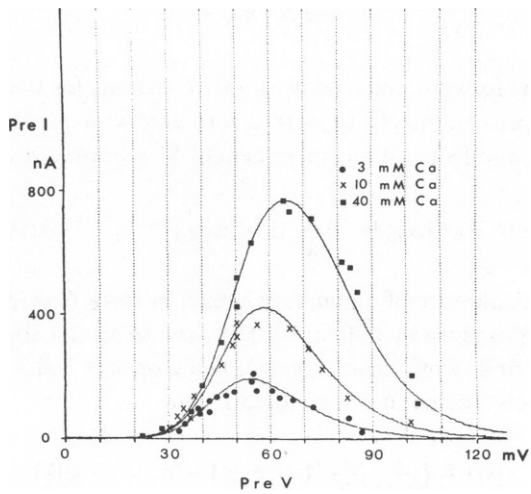

FIGURE 14 Plot of experimental values for $\bar{I}_{Ca}$ at 3, 10, and 40 mM $[Ca^{2+}]_o$ (symbols) and comparison with results obtained from numerical solutions to Eq. 17 (solid lines). Note the shift of peak $\bar{I}_{Ca}$ to the right with increased $[Ca^{2+}]_o$.

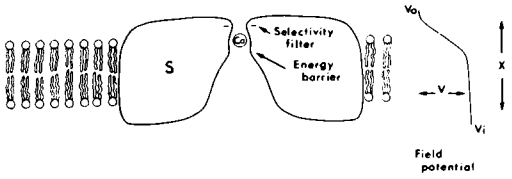

FIGURE 15 Schematic diagram of the hypothetical calcium channel. The channel is envisioned as a protein moiety comprised of five subunits (S) which delimit a pore through the lipid-bilayer membrane. An energy barrier for ionic movement is expected to be located near the outer surface of the membrane (top of figure). A negatively charged selectivity filter must be present and is shown in the external opening of the channel. Our results imply that the voltage drop along the channel occurs across the external portion of the channel. For details, see text.

tail current amplitude. This result was corroborated by measurements of the instantaneous tail current, which demonstrated that this voltage dependence could not be described by a constant field. Thus, we now assume that the potential drop is nonlinearly distributed across the length of the ion channel (Fig. 15) as will be described below.

This nonlinear behavior could also be explained in terms of saturation of the ionic channel, or as an asymmetry due to current moving from an area of high concentration to one of low concentration (cf. Dodge and Frankenhaeuser, 1959). In formulating our model, we have included all three points. A model was thus developed which accounts for the empirical data and otherwise resembles in general lines, that of Hodgkin and Huxley (1952 *c*) for the potassium current.

CHANNEL OPENING AND CLOSING It is assumed that each calcium channel is composed of n subunits, each of which may be in one of two forms, S or S', the gate being open if all n subunits are in the S' form. No mutual influence on the S or S' forms of a subunit by its neighbors is assumed. The system may thus be described by the following scheme:

$$S \underset{k_2}{\overset{k_1}{\rightleftharpoons}} S';\ nS' \leftrightarrow G,$$

where k_1 and k_2 are the forward and backward rate constants for the conversion of S into S', and G designates an open channel. If we start at zero time with a system in which no channels are open, i. e. $[G] = 0$, and $[S'] = 0$, the increment of S' with time will be given by:

$$[S'] = [S]_0 \frac{k_1}{k_1 + k_2}\{1 - \exp[-(k_1 + k_2)t]\}, \tag{3}$$

where $[S]_o$ is the total number of subunits whether in form S or S'. The probability of a subunit to be in form S' is given by $[\bar{S}] = [S']/[S]_o$, and of having all its subunits (n) in the S' form is $[\bar{S}]^n$. The probability of a given channel being open is $[\bar{G}] = [G]/[G]_o$. ($[G]_o$ is the total number of channels whether open or closed.) Thus:

$$[\bar{G}] = \left(\frac{k_1}{k_1 + k_2}\{1 - \exp[-(k_1 + k_2)t]\}\right)^n. \tag{4}$$

Since I_{Ca} is potential-dependent (Figs. 8–10), so are k_1 and k_2. Such a dependence may occur if the charge distribution in S or S' is different from that of the activated transition state for

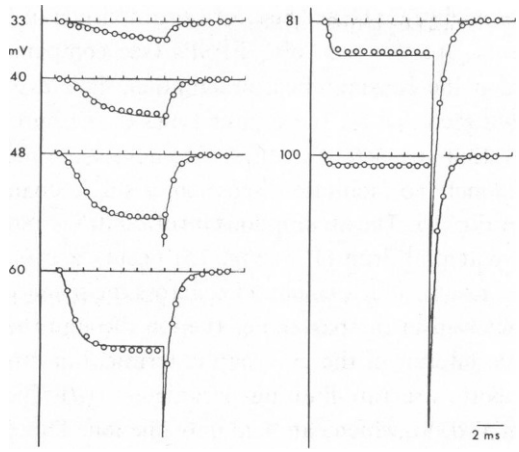

FIGURE 16 Comparison of experimentally recorded I_{Ca} (open circles) with numerical solution of Eq. 15 (solid lines) for the same voltage steps. While the time course is similar for the two sets of results, some difference in amplitude is seen in the tail currents above 60 mV where the experimental data falls short of the model. (Data from currents in Fig. 8 *A*).

the S to S' transformation. The contribution of the membrane potential, V, to the energies of activation of the reactions corresponding to k_1 and k_2 will be given by $z_1\epsilon V = (p - p_1)V/m$ and $z_2\epsilon V = (p - p_2)V/m$, respectively, where ϵ is the elementary electric charge, m is the thickness of the membrane across which the potential drops; p, p_1, and p_2 are the component of the dipole moments (exposed to the membrane electric field and perpendicular to the membrane plane) of the activated transition state, and of S and of S', respectively. The symbols z_1 and z_2 designate the respective number of charges that will move across the width of the membrane on transforming S and S' into the activated transition state to produce an equivalent dependence on V. Although z_1 and z_2 may be voltage-dependent, holding these values constant allows a reasonable fit to the data while keeping the number of voltage-dependent variables to a minimum (see Figs. 9 and 16). The dependence of k_1 and k_2 on V will thus be:

$$k_1 = k_1^\circ \exp(\epsilon z_1 V/kT);\ k_2 = k_2^\circ \exp(\epsilon z_2 V/kT), \tag{5}$$

where k_1° and k_2° do not depend on the membrane potential[1], k is Boltzmann's constant, and T the absolute temperature (291°K = 18°C). V is expressed with reference to absolute zero potential.

CALCULATION OF INWARD CALCIUM CURRENT; THE QUESTION OF DISTRIBUTION OF ELECTRIC FIELD ALONG THE CALCIUM CHANNEL I_{Ca} is determined by the number of open channels $[G]$ at the moment of interest (t), multiplied by the flow of calcium ions per unit time

[1] k_1° and k_2° may depend on temperature (T). If $\Delta H_1^\dagger$ and $\Delta H_2^\dagger$ are the respective enthalpies of activation, the following is expected to hold:

$$k_1^\circ = k_1^{\infty} \exp(-\Delta H_1^\dagger/kT);\ k_1^\circ = k_2^{\infty} \exp(-\Delta H_2^\dagger/kT), \tag{6}$$

where k_1^∞ and k_2^∞ are constants that depend neither on V nor on T. The temperature dependence of k_1 and k_2 will thus be governed both by the membrane potential and the enthalpies of activation.

through a single open channel (j). To account for the amplitude of (a) the tail currents, (b) the instantaneous currents, and (c) the "off" EPSPs (see companion paper, Llinás et al., 1981), we had to abandon the constant field assumption. This assumption predicts values approximately twice those recorded for these three types of measurements (see inset in Fig. 17). Instead, we assume that the potential difference across the membrane is limited to a certain region of the channel. To facilitate discussion, a single channel may be pictured in cross-section as shown in Fig. 15. The assumptions involved in the model of the channel itself are as follows: (a) The potential drop (V in Fig. 15) occurs across a fraction of the outer channel length. (b) The movement of a calcium ion across the potential drop is fast compared to the other processes involved in the passage of the ion through the channel. (c) Diffusion from the channel into the interior of the presynaptic terminal or crossing an energy barrier within the channel, or both, are rate-limiting parameters. (d) There is a site within the channel, after the potential drop, which can hold only one ion. This could be the recognition site for calcium. (One could generalize the model to a site that can hold more than one ion, but this was not found to be necessary.) The fractional number of sites occupied by a calcium ion is designated $[P]$. It follows then that there is a saturation of the ionic channels. (e) The channel contains a selectivity filter; however, the model is independent of its location. It stands to reason nevertheless that it should be located near the external entrance of the channel (see Fig. 15).

The treatment of the case in which the potential drop is located at the external face of the channel was found to account for our data. For such a case one can write for j, the rate of flow through a single channel:

$$j = \beta_1[P] - \beta_2 dc_i(1 - [P]), \tag{7}$$

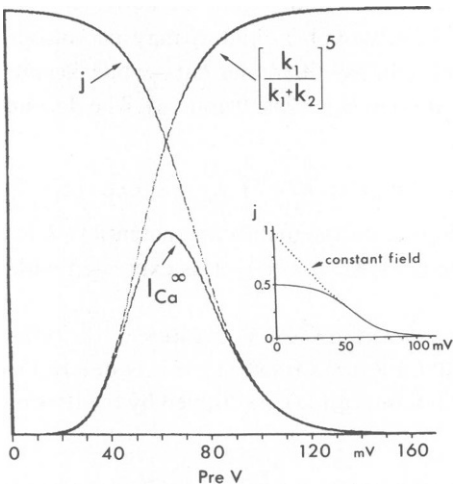

FIGURE 17 Contribution of the current flow per open channel (j, which is proportional to $[P]$ since β_1 is a constant) and the number of open channels (given by $[k_1/k_1 + k_2]^5$) to the determination of I_{Ca}^{∞} as a function of V (Eq. 17). (*inset*) comparison of j assuming a constant (dots) and a nonuniform (solid line) field across the length of the calcium channel. $[Ca^{2+}]_o$ = 10 mM.

where c_i is a compact notation equivalent to $[Ca^{2+}]_i$, the internal calcium concentration, β_1 and β_2 are proportionality factors, and d expresses the distribution factor of calcium between the cytoplasm and the channel. Following our assumptions, we write for $[P]$ an equilibrium expression,

$$\frac{[P]}{(1 - [P])c_0} = K \exp(-2\epsilon V/kT) = K \exp(-80\ V) \tag{8}$$

$$\therefore [P] = \frac{Kc_0 \exp(-80\ V)}{1 + Kc_0 \exp(-80\ V)}, \tag{9}$$

where c_o is a compact equivalent of $[Ca^{2+}]_o$, the external calcium concentration, and K is an equilibrium constant. For small and intermediate depolarizations, at which $[P]$ is not small compared to $1 - [P]$, one can ignore the term containing c_i in Eq. 7, and thus obtain:

$$j = \beta_1 \frac{Kc_0 \exp(-80\ V)}{1 + Kc_0 \exp(-80\ V)}. \tag{10}$$

At high depolarizations which approach E_{Ca}, one should use the complete expression:[2]

$$j = \beta_1 \frac{K[c_0 \exp(-80\ V) - c_i]}{1 + Kc_0 \exp(-80\ V)} = \beta_1 [F], \tag{14}$$

where $[F]$ gives the driving force. This expression is then similar to the traditional formulation where current is equal to driving force (a function of voltage and ionic concentration) and conductance (a constant). This expression includes the effect of current inversion at very high depolarizations. Note that this equation incorporates an asymmetry which is due both to current moving between areas of different concentrations (cf. Dodge and Frankenhaeuser, 1959) and to the structural asymmetry of the channel.

CALCIUM FLOW AS A FUNCTION OF TRANSMEMBRANE VOLTAGE The calcium current (I_{Ca}) flowing into the presynaptic terminal is obviously the product of the number of open channels at the moment of interest, t, and the current flow per channel, i.e.,

---

[2]At the equilibrium potential for calcium, the following holds:

$$\frac{c_i}{c_0} = \exp(-80\ V) \text{ and } j = 0 = \beta_1 [P] - \beta_2\, dc_i(1 - [P]). \tag{11}$$

From the second expression, we get:

$$\frac{\beta_2 dc_i}{\beta_1} = \frac{[P]}{1 - [P]} = Kc_0 \exp(-80\ V) = Kc_0 \frac{c_i}{c_0} = Kc_i, \tag{12}$$

$$\beta_2 d = \beta_1 K.$$

Therefore,

$$j = \beta_1([P] - Kc_i(1 - [P])) = \frac{\beta_1 K[c_0 \exp(-80\ V) - c_i]}{1 + Kc_0 \exp(-80\ V)}. \tag{13}$$

$$I_{ca} = [G] \cdot j = [G]_0 \cdot \left(\frac{k_1}{k_1 + k_2}\{1 - \exp[-(k_1 + k_2)t]\}\right)^n \cdot \frac{\beta_1 K[c_0 \exp(-80\ V) - c_i]}{1 + Kc_0 \exp(-80\ V)}. \quad (15)$$

Eq. 15 was plotted for various values of the parameters (n, z_1, z_2) (Llinás et al., 1976) and after comparison with the experimental results, we arrived at values of $n = 5$, $k_1° = 2.76\ \text{ms}^{-1}$; $k_2° = 0.14\ \text{ms}^{-1}$; $z_1 = 1.42$; $z_2 = -0.38$; and $K = 35\ \text{M}^{-1}$. These values are used throughout in solving all the equations. The numerical solution for Eq. 15 giving time course and amplitude of I_{Ca} are presented in Figs. 9 and 16 for different levels of voltage clamp depolarization. The agreement with the experimental data is apparent. Note in Fig. 16 that while the "on" current agree well with the model, the tail currents at high depolarization clamps are somewhat smaller than those expected from the model. See also Fig. 11 *C* and *D*.

INSTANTANEOUS CURRENTS Starting from a common (in this case, depolarized) voltage, V_I, and clamping to any second voltage, V_{II}, one assumes that at the moment of the voltage transition [G] has a common value since it has not yet changed to that appropriate to the new voltage. Hence, the instantaneous current amplitudes are proportional to j; and the instantaneous current should be proportional to the function:

$$j = \frac{\beta_1 K[c_0 \exp(-80\ V_{II}) - c_i]}{1 + Kc_0 \exp(-80\ V_{II})}. \quad (16)$$

where V_{II} is the membrane potential in absolute units. Note that the internal and external calcium concentrations (c_i and c_o, respectively) enter this expression.

The numerical solution of Eq. 16, giving the current per channel as a function of clamp voltage at 10 mM external calcium concentration is given by the solid line in Fig. 12 and is shown for different calcium concentrations in the inset. The fit with experimental data for five synapses at 10 mM $[Ca^{2+}]_o$ is reasonable, which is to be expected if the current-voltage relationship for any number of open channels has the same shape as that of a single open channel.

STEADY-STATE CALCIUM FLOW AND CALCIUM CONCENTRATION To look at the voltage dependence of I_{Ca}, an expression for the steady-state I_{Ca} is necessary. These values are readily obtained from Eq. 15 with $n = 5$ and by setting t to ∞:

$$I_{Ca}^{\infty} = [G]_0 \left(\frac{k_1}{k_1 + k_2}\right)^5 \cdot \frac{\beta_1 K[c_0 \exp(-80\ V) - c_i]}{1 + Kc_0 \exp(-80\ V)} \quad (17)$$

The solution to Eq. 17 was plotted for various values of V in Figs. 10, 11 *C* and *D*, 14, and 17 ($c_o = 10$ mM). Agreement between the solution to Eq. 17 and the data is good, the most variation being seen at the higher voltages. To learn how this relationship changes with $[Ca^{2+}]_o$, Eq. 17 was plotted for various values of V at $c_o = 3$, 10, and 40 mM. As shown in Fig. 14, the current onset is not affected significantly although the peak current moves to the right with increasing $[Ca^{2+}]_o$ as does E_{Ca}.

The relative contribution of j (the current flowing through an open channel) and the number of open channels (given by $[k_1/(k_1 + k_2)]^5$) to I_{Ca}^{∞} for various levels of membrane depolarization is shown in Fig. 17. As can be seen, for low levels of depolarization the term

$[k_1/(k_1 + k_2)]^5$ is low and thus the limiting factor; however, at ~60 mV depolarization as the driving force diminishes, the number of open channels is still increasing and thus j is the limiting factor and determines the shape of the falling phase of the curve.

At high depolarizations the contribution of c_i to j cannot be ignored, especially since there may be an appreciable increase in $[Ca^{2+}]_i$ at the channel's surface. Sample cases were run to determine how $[Ca^{2+}]_i$ of 10^{-3}–10^{-4} M could affect the shape of I_{Ca}^{∞} vs. V, and it was found, as expected, that c_i affects j only at high levels of presynaptic depolarization that approach E_{Ca} (not shown). At such depolarizations, however, I_{Ca} (and hence c_i) is rather small.

CALCIUM CURRENTS AND CONDUCTANCES DURING PRESYNAPTIC ACTION POTENTIAL Eq. 15 cannot be utilized directly to evaluate the time course of I_{Ca} when the membrane potential is not constant since this equation supposes that k_1 and k_2 are constant with time. As shown above, however, k_1 and k_2 will vary with time if the membrane potential changes. Under such circumstances the following procedure may be adopted. Thus, if

$$S \underset{k_2}{\overset{k_1}{\rightleftharpoons}} S', \text{ then}$$

$$\frac{d[\bar{S}]}{dt} = -(k_1 + k_2)[\bar{S}] + k_1 \ . \tag{18}$$

This equation can be integrated numerically in a stepwise way with k_1 and k_2 varying with time. $[\bar{G}]$ is then obtained from $[\bar{G}] = [\bar{S}]^5$ and I_{Ca} is obtained from $I_{Ca} = [G] \cdot j$. The solution to Eq. 18 is shown at the bottom of Fig. 18, which illustrates the time course and amplitude of I_{Ca} generated during an action potential implemented according to the Hodgkin and Huxley model (1952 *d*).

Regarding the calculation of g_{Ca}, an analysis of the instantaneous currents (Fig. 12) shows that the resistance of an open channel is far from ohmic. That is, the calcium flow through an open channel is not directly proportional to voltage since, due to the special structure of this channel, $[P]$ is voltage-dependent but in a highly nonlinear fashion (see Eq. 9). Thus, β_1 can be taken as a measure of the calcium conductance of a single open channel. It is given by:

$$\beta_1 = \frac{j}{[F]} = j \cdot \left\{ \frac{K[c_0 \exp(-80\ V) - c_i]}{1 + Kc_0 \exp(-80\ V)} \right\}^{-1} . \tag{19}$$

The calcium conductance of the membrane is therefore:

$$g_{Ca} = \beta_1 \cdot [G]. \tag{20}$$

Historically, ionic conductances have been expressed as the ratio of current to driving force; for this reason we have calculated the calcium conductance not using Eq. 20 but rather adopting the Hodgkin-Huxley formulation for an action potential (upper part of Fig. 18). This was done for the sake of comparison to other calcium conductance (Akaike et al., 1978; Adams and Gage, 1979) and is only correct if the conductance is expressed for a given membrane potential value, given the nonlinear relation between V and driving force. It must be clear, on the other hand, that if Eq. 20 were to be used, the estimated "conductances," given their respective definitions, could have different numerical values. In either case, to obtain I_{Ca} from the conductance, the conductance must be multiplied by the corresponding

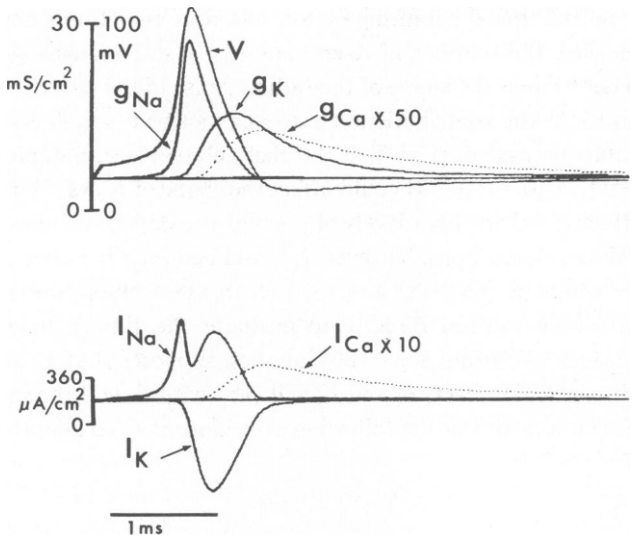

FIGURE 18 Action potential. Upper record, action potential reconstructed from Hodgkin-Huxley equations, including the values for g_{Na} and g_K. g_{Ca} is expressed as the ratio of current to driving forces. Lower record, current density for these three currents obtained from Hodgkin-Huxley equation and our Eq. 18.

driving force. This will be membrane potential in the Hodgkin-Huxley formulation and $[F]$ in this model (Eqs. 19 and 20). However, the actual value for I_{Ca} will be the same regardless of the definition of conductance one chooses to use.

DISCUSSION

The aim of the present paper is to provide a quantitative description of the voltage-dependent calcium conductance changes at the presynaptic terminal in the squid giant synapse. Based on voltage clamp results, a kinetic model has been constructed which describes these voltage- and time-dependent conductance changes. The model assumes the calcium current in this terminal to be brought about by a mechanism similar to that suggested for the sodium and potassium currents in squid nerve (Hodgkin and Huxley, 1952 *c*) and in other excitable tissue (Hille, 1975); i.e., a voltage gating of ion-specific transmembrane channels.

Voltage and Time Dependence of the Calcium Conductance

The voltage-dependent calcium conductance change at the presynaptic terminal of the squid giant synapse may be described as having three major characteristics. Thus, as previously concluded from the direct measurement of calcium influx with aequorin (Baker et al., 1971; Llinás and Nicholson, 1975) as well as from other experiments (cf. Blinks et al., 1976), the voltage-dependent calcium conductance change is typified by (*a*) a rather slow onset which has a sigmoidal time course, (*b*) the lack of a fast inactivation, and (*c*) the presence of a sizeable tail current, which is particularly clear when the voltage clamp level reaches sufficient depolarization to significantly reduce the calcium driving force during the pulse. While these findings are in some respects similar to those reported for other cells including

amphibian twitch muscle (Sanchez and Stefani, 1978), mammalian cardiac muscle (New and Trautwin, 1972), crustacean muscle (Keynes et al., 1973; Hencek and Zachar, 1977; Hagiwara et al., 1974); squid axon (Baker et al., 1973; Meeves and Vogel, 1973), molluscan nerve cell bodies (Geduldig and Gruener, 1970; Standen, 1975; Eckert and Lux, 1976; Kostyuk and Krishtal, 1977; Akaike et al., 1978 *a* and *b*; Lee et al., 1978; Connor, 1979; Lux and Heyer, 1979), and unfertilized tunicate egg membrane (Okamoto et al., 1976), there are reported differences between these calcium conductances as related to E_{Ca}, and activation and inactivation kinetics.

IDENTIFICATION OF THE INWARD CURRENT Pharmacological isolation of the calcium conductance has been made possible by the introduction in the superfusion fluid of sufficient TTX to produce a rather complete blockage of peak sodium conductance and enough intracellular TEA and extracellular 3- or 4-aminopyridine to block almost completely the voltage-dependent potassium conductance. The possibility that a calcium-dependent potassium conductance change may mask or modify the time course of the inward current seems unlikely, at least for the short duration of our voltage pulses. Indeed, it seems clear that in this preparation, after the above pharmacological treatment, the calcium-dependent potassium conductance could be quite late since, when observable (<10% of experiments), it is evident with voltage pulses of >7 ms duration as is the case with similar conductances in other systems (cf. Meech, 1978; Lux and Heyer, 1979). The late slow inward current is blocked by the addition of manganese, cadmium, or cobalt to the bath or by lowering $[Ca^{2+}]_o$ to 0.5 mM. We conclude, therefore, that the inward current which we observed after blockage of the voltage-dependent sodium and potassium currents is carried mainly by calcium ions.

TIME COURSE AND AMPLITUDE OF I_{Ca} The calcium conductance change in the preterminal is characterized by a sigmoidal time course whose rate of rise and amplitude are voltage-dependent. As seen in Figs. 8 and 9, the maximum rate of rise of the calcium current, as indicated previously (Llinás et al., 1976) was reached near 62 mV from resting (i.e., -8 mV, the holding potential being -70 mV) and the maximum amplitude at ~60 mV (for 10 mM $[Ca^{2+}]_o$). The amplitude then decreased to a negligible value above 140 mV from resting (i.e., +70 mV). The plateau values for inward calcium current (I_{Ca}^{∞}) were plotted as a function of voltage in Figs. 10, 11 *C*, and 14. As expressed by our model, and as will be discussed further below, this bell-shaped curve may be accurately described as the product of the voltage-dependent conductance change and the driving force for calcium ($[F]$). The voltage dependence of g_{Ca}, as defined by Eq. 20, is sigmoidal and reached close to saturation near 100 mV (for 10 mM $[Ca^{2+}]_o$), the driving force being maximum at rest and decreasing with voltage (see Fig. 17)

LACK OF FAST INACTIVATION RESPONSE Although calcium channel inactivation has been proposed to exist in several tissues including molluscan cells (Adams and Gage, 1979; Kostyuk and Krishtal, 1977), tunicate egg membrane (Okamoto et al., 1976), muscle (Keynes et al., 1973; Hagiwara et al., 1974; Sanchez and Stefani, 1978), skate electroreceptor (Clusin and Bennett, 1977) and squid axon (Baker et al., 1971), for the most part, this inactivation is relatively slow and, in some cases, incomplete. The present studies agree, for the most part, with the data by Baker et al. (1971) in the squid giant axon in the sense that calcium inactivation in these fibers may occur only very slowly. A similar conclusion was obtained by indirect means by Katz and Miledi (1971) relating to the decrease observed in the plateau of

the calcium action potential during prolonged depolarizations. While on several occasions an apparent inactivation of calcium current was seen in our experiments, it could be demonstrated, in every case, that this sham inactivation was produced by a remaining voltage-dependent potassium conductance contaminating the inward calcium current trace. However, even in those cases where an outward current was observed, synaptic transmission continued during this outward current (see Fig. 6) and blockage of the calcium channels by addition of 1 mM cadmium demonstrated that this early outward voltage-dependent current was independent of the calcium current. Based on the above, and in accordance with related findings such as the presence of prolonged all-or-none calcium spikes in this preparation (Katz and Miledi, 1971; Llinás et al., 1976) and prolonged synaptic transmission in other preparations (Blight and Llinás, 1980), we assume that for durations relevant to this set of experiments, calcium inactivation was negligible.

Tail Current

The absence of inactivation is further supported by the tail current measurements. The amplitudes of the tail current—especially those following voltage clamp steps close to E_{Ca}—are quite close to values obtained by our model (which does not include inactivation), indicating that no significant inactivation of this current occurred during the period of the voltage step (see Figs. 11 and 16). In addition to providing direct evidence for the lack of calcium channel inactivation, tail current measurements provided important information regarding the time constant of closure of calcium channels. The time course of the tail currents could be described by a single exponential, indicating that the rate for channel closure followed first-order kinetics. As will be seen below, study of the instantaneous currents was of help in determining the value for the current through single channels and indicated that this current was not subject to a constant field, as it saturated at high membrane potentials and calcium concentrations. Indeed the agreement between the instantaneous currents and the values predicted by our model (Fig. 12) is quite good, at least within the level of experimental error, and supports the assumption of the nonconstant field properties for this calcium channel.

Calcium Equilibrium Potential

The measurement of an equilibrium potential has been one of the most useful experimental tools in characterizing transmembrane ionic conductances. This most sensitive measurement underlies one of the crucial concepts from which the ionic conductance hypothesis of nerve impulse was generated (cf. Cole, 1968). The concept, however, is useful and applicable only in situations where the concentration of the ion carrying the current is comparably high on both sides of the membrane. In such a case, a clear reversal of the direction of current flow, as the membrane voltage goes beyond the equilibrium potential for the ion in question, may occur. As previously reported in squid presynaptic terminal (Llinás et al., 1976) and confirmed for molluscan cells (Akaike et 1978 *b*), and in tunicate egg membrane (Okamoto et al., 1976), in the case of calcium currents, a reversal was not present. In fact, for depolarizations beyond 140 mV, I_{Ca} is not measurable, at least in the sense that the outward I_{Ca} (if at all present, given the low $[Ca^{2+}]_i$) is extremely small. Indeed, solution of Eq. 15 indicates that a reversal potential for calcium is only to be expected if the intracellular concentration were to be maintained at a level of at least 10^{-4} M. As expected, therefore, our results demonstrate,

rather than a reversal potential, an asymptotic approach toward a zero calcium current. (According to the model the actual reversal would occur at 226 mV from rest; rest = -70 mV; $[Ca^{2+}]_o = 10^{-3}$ M; $[Ca^{2+}]_i = 10^{-7}$ M.) This being the case, one must assume that those experiments in which a reversal of the so-called calcium current has been seen may be due to the poor condition of the cells, allowing elevated levels of $[Ca^{2+}]_i$, or due to contamination by outward currents carried most probably by potassium rather than representing an outward calcium current.

Kinetic Model

One of the main motives in attempting a voltage clamp study was to determine the properties of I_{Ca} to develop a mathematical model which would allow a prediction of calcium currents and a further understanding of the role of calcium in synaptic transmission itself. Given this goal, a kinetic model should not only be consistent with the voltage clamp data but should be predictive as well.

The model presented here assumes that the calcium conductance is brought about by the opening of a channel comprised of five subunits. Each subunit undergoes an independent change following first-order kinetics that resemble in some ways the n^4 gate kinetics originally described by Hodgkin and Huxley (1952 *c*) for the potassium current. In our case, however, rather than a fourth order, a fifth order kinetic relationship fit the data best, although in fact we cannot distinguish reliably between an $n = 5$ and $n = 6$ (Llinás et al., 1976). In this respect, our results are quite similar to those obtained subsequently by Hencek and Zachar (1977) in crustacean muscle fibers where sixth order kinetics were found.

Concerning the resistive properties of single channels, the rate-limiting step determining ionic flow in our case was not the electric field itself, but rather was determined by two other factors, (*a*) the binding or delay of ions within the channel, and/or (*b*) the ease with which they diffuse away from the binding site. The latter point may be significant, given that the calcium diffusion constant at the site of entry into the cytoplasmic milieu may differ from that in the channel itself, and may thus represent a resistance in series.

Other points arising from the model relate single channel conductance to extracellular calcium and extracellular calcium concentration to calcium current.

The present model is complementary to the suggestion put forth for the calcium conductance in barnacle muscle by Hagiwara and Takahashi (1967) and in *Helix* neurons by Akaike et al. (1978 *a* and *b*) in which it is speculated that the calcium channel may contain a voltage-dependent site which binds divalent cations.

I_{Ca} and g_{Ca} during a Presynaptic Action Potential

Of central interest to an understanding of synaptic transmission itself was the attempt to determine the time course for I_{Ca} during a normal presynaptic action potential. This was done by solving equations for a nonsquare voltage change across the membrane (Fig. 18). Our results suggest that in the presynaptic terminal I_{Ca} lags and has an amplitude of $\sim 1/20$ of the sodium current per unit membrane. Calculation of the currents flowing through these different channels was generated by coupling the Hodgkin-Huxley equations with our own for the calcium current. The results in the lower part of Fig. 18 indicate that the peak current density would be $\sim 42\ \mu A/cm^2$. These results assume a total area of $\sim 12.56 \times 10^{-4}\ cm^2$ for the presynaptic digit (25 μm in radius and 800 μm in length). The question of whether this result

relates to any actual physical structure cannot be determined at this time. However, for the purposes of this discussion, we may assume that calcium currents may flow through particular structures in the subsynaptic membrane (Llinás and Heuser, 1977). In fact, a freeze-fracture study of the presynaptic terminal in the squid synapse (see Pumplin and Reese, 1978) suggests that, as originally proposed for the neuromuscular junction, the rather large particles observed at the active zone in this synapse may represent such calcium channels. Assuming that these particles represent transmembrane channels, if a chord conductance were to be estimated for this terminal $[I_{Ca}/(V-E_{Ca})$ assuming a value of 180 mV for $E_{Ca}]$ and this value divided by the average number of channels per synapse, the conductance per unit channel would fall within 10^{-13} and 10^{-14} *S*, a value quite similar to that observed by Akaike et al. (1978) in *Helix* neurons.

In short, our results lend support to the suggestion that the transmembrane particles observed by Pumplin and Reese (1978) may represent channels for the movement of calcium ions across the membrane. While this must continue to be a hypothetical and but one of the possible physical representations of the channel, it may prove to be a useful concept, especially as the search for calcium channels begins to take shape.

Finally, one of the clear predictions from the model is that calcium conductance occurs rather late during the action potential, at a time when the driving force for calcium is considerable, given that the membrane potential has, at that time, returned to close to its resting value. In addition, as the calcium current appears at the falling phase of the action potential, synaptic transmission is basically generated by an "off" calcium current. This will give the postsynaptic potential the rather fast rate of rise which characterizes chemical transmission in most ionophoric synapses.

Mr. Michio Chujo was of invaluable help in writing the computer programs and obtaining the numerical solutions described in this and the subsequent paper. We would like to thank our colleague B. Rudy for his comments on the manuscript and M. Sugimori and S. M. Simon for collaboration in recent experiments. Research was supported by U. S. Public Health Service grant NS-13742 from the National Institute of Neurological and Communicative Disorders and Stroke.

Received for publication 15 October 1980.

REFERENCES

ADAMS, D. J., and P. W. GAGE. 1979. Characteristics of sodium and calcium conductance changes produced by membrane depolarization in an *Aplysia* neurone. *J. Physiol. (Lond.).* **289**:143–161.

ADRIAN, R. H., W. K. CHANDLER, and A. L. HODGKIN. 1970. Voltage clamp experiments in striated muscle fibers. *J. Physiol. (Lond.).* **208**:607–644.

AGIN, D. P. 1969. Electrochemical properties of glass microelectrodes. *In* Glass Microelectrodes. M. Lavalle, O. F. Schanne, and N. C. Hebert, editors. John Wiley & Sons, New York. 62–75.

AKAIKE, N., H. M. FISHMAN, K. S. LEE, L. E. MOORE, and A. M. BROWN. 1978 *a*. The units of calcium conduction in *Helix* neurones. *Nature (Lond.).* **274**:379–381.

AKAIKE, N., K. S. LEE, and A. M. BROWN. 1978 *b*. The calcium current of *Helix* neuron. *J. Gen. Physiol.* **71**:509–531.

ALNAES, E., and R. RAHAMIMOFF. 1975. On the role of mitochondria in transmitter release from motor-nerve terminals. *J. Physiol. (Lond.).* **248**:285–306.

ARMSTRONG, C. M., and L. BINSTOCK. 1965. Anomalous rectification in the squid giant axon injected with tetraethylammonium chloride. *J. Gen. Physiol.* **48**:859–872.

AUERBACH, A. A., and M. V. L. BENNETT. 1969. Chemically mediated transmission at a giant fiber synapse in the central nervous system of a vertebrate. *J. Gen. Physiol.* **53**:183–210.

BAKER, P. F., A. L. HODGKIN, and E. B. RIDGWAY. 1971. Depolarization and calcium entry in squid giant axons. *J. Physiol. (Lond.).* **218**:709–755.

BAKER, P. F., H. MEVES, and E. B. RIDGWAY. 1973. Calcium entry in response to maintained depolarization of squid axons. *J. Physiol. (Lond.).* **231**:527–548.

BLAUSTEIN, M. P., E. M. JOHNSON, and P. NEEDLEMAN. 1972. Calcium-dependent norepinephrine release from presynaptic nerve endings *in vitro*. *Proc. Natl. Acad. Sci. U.S.A.* **69**:2237–2240.

BLIGHT, A. R., and R. LLINÁS. 1980. The non-impulsive stretch-receptor complex of the crab: a study of depolarization-release coupling at a tonic sensorimotor synapse. *Phil. Trans. R. Soc. Lond. B Biol. Sci.* **290**:219–276.

BLINKS, J. R., F. G. PRENDERGAST, and D. G. ALLEN. 1976. Photoproteins as biological calcium indicators. *Pharmacol. Rev.* **28**:1–93.

BROWN, K. T., and D. G. FLAMING. 1977. New microelectrode techniques for intracellular work in small cells. *Neuroscience* **2**:813–827.

CHANDLER, W. K., R. F. RAKOWSKI, and M. F. SCHNEIDER. 1976. A nonlinear voltage-dependent charge movement in frog skeletal muscle. *J. Physiol. (Lond.).* **254**:245–283.

CLUSIN, W. T., and M. V. L. BENNETT. 1977. Calcium-activated conductance in skate electroreceptors: voltage clamp experiments. *J. Gen. Physiol.* **69**:145–182.

COLE, K. S. 1949. Dynamic electrical characteristics of the squid axon membrane. *Arch. Sci. Physiol.* **3**:253–258.

COLE, K. S. 1968. Membranes, Ions, and Impulses. Univ. of California Press, Berkeley, Calif.

CONNOR, J. A. 1979. Calcium current in molluscan neurons: measurement under conditions which maximize its visability. *J. Physiol. (Lond.).* **286**:41–60.

DI POLO, R., J. REQUENA, F. J. BRINLEY, Jr., L. J. MULLINS, A. SCARPA, and T. TIFFERT. 1976. Ionized calcium concentration in squid axons. *J. Gen. Physiol.* **67**:433–467.

DODGE, F. A., and B. FRANKENHAEUSER. 1959. Sodium currents in the myelinated nerve fiber of *Xenopus laevis* investigated with the voltage clamp technique. *J. Physiol. (Lond.).* **148**:188–200.

ECKERT, R., and H. D. LUX. 1976. A voltage-sensitive persistent calcium conductance in neuronal somata of Helix. *J. Physiol. (Lond.).* **254**:129–151.

GEDULDIG, D., and R. GRUENER. 1970. Voltage clamp of the *Aplysia* giant giant neurones: early sodium and calcium currents. *J. Physiol. (Lond.).* **211**:217–244.

GRAUBARD, K., and W. H. CALVIN. 1979. Presynaptic dendrites: Implications of spikeless synaptic transmission and dendritic geometry. *In* The Neurosciences: Fourth Study Program. F. O. Schmitt and F. G. Worden, editors. M.I.T. Press, Cambridge, Mass. 317–331.

HAGIWARA, S., J. FUKUDA, and D. C. EATON. 1974. Member currents carried by Ca, Sr, and Ba in barnacle muscle fiber during voltage clamp. *J. Gen. Physiol.* **63**:564–578.

HAGIWARA, S., and S. NAKAJIMA. 1966. Differences in Na and Ca spikes as examined by application of TTX, procaine, and manganese ions. *J. Gen. Physiol.* **49**:793–806.

HAGIWARA, S., and K. TAKAHASHI. 1967. Surface density of calcium ions and calcium spikes in the barnacle muscle fiber membrane. *J. Gen. Physiol.* **50**:583–601.

HENCEK, M., and J. ZACHAR. 1977. Calcium currents and conductances in the muscle membrane of the crayfish. *J. Physiol. (Lond.).* **268**:51–71.

HILLE, B. 1975. Ionic selectivity of Na and K channels of nerve membranes. *In* Membranes: A Series of Advances, Vol. 3. G. Eisenman, editor. Marcel Dekker, Inc., New York. 255–323.

HODGKIN, A. L., and A. F. HUXLEY. 1952 *a*. The components of membrane conductance in the giant axon of *Loligo*. *J. Physiol. (Lond.).* **116**:449–472.

HODGKIN, A. L., and A. F. HUXLEY. 1952 *b*. Currents carried by sodium and potassium ions through the membrane of the giant axon of *Loligo*. *J. Physiol. (Lond.).* **116**:449–472.

HODGKIN, A. L., and A. F. HUXLEY. 1952 *c* A quantitative description of membrane current and its application to conduction and excitation in nerve. *J. Physiol. (Lond.).* **117**:500–544.

HODGKIN, A. L., A. F. HUXLEY, and B. KATZ. 1952. Measurement of current-voltage relations in the membrane of the giant axon of *Loligo*. *J. Physiol. (Lond.)* **116**:424–448.

KASS, R. S., S. A. SIEGELBAUM, and R. W. TSIEN. 1979. Three-microelectrode voltage clamp experiments in calf cardiac Purkinje fibers. Is slow inward current adequately measured? *J. Physiol. (Lond.).* **290**:201–225.

KATZ, B. 1969. The Release of Neural Transmitter Substances. Charles C. Thomas, Springfield, Ill.

KATZ, B., and R. MILEDI. 1967. A study of synaptic transmission in the absence of nerve impulses. *J. Physiol. (Lond.).* **192**:407–436.

KATZ, B., and R. MILEDI. 1969 *a*. Tetrodotoxin-resistant electric activity in presynaptic terminals. *J. Physiol. (Lond.).* **203**:459–487.

KATZ, B., and R. MILEDI. 1969 *b*. The effect of divalent cations on transmission in the squid giant synapse. *Publ. Staz. Zool. Napoli.* **37**:303–310.

KATZ, B., and R. MILEDI. 1970. Further study of the role of calcium in synaptic transmission. *J. Physiol. (Lond.).* **207**:789–801.

KATZ, B., and R. MILEDI. 1971. The effect of prolonged depolarization on synaptic transfer in the stellate ganglion of the squid. *J. Physiol. (Lond.).* **216**:503–512.

KEYNES, R. D., E. ROJAS, R. E. TAYLOR, and J. VERGARA. 1973. Calcium and potassium systems of a giant barnacle muscle fiber under membrane potential control. *J. Physiol. (Lond.).* **229**:409–455.

KOSTYUK, P. G., and O. A. KRISHTAL. 1977. Separation of sodium and calcium currents in the somatic membrane of mollusc neurones. *J. Physiol. (Lond.).* **270**:545–568.

KUSANO, K. 1970. Influence of ionic environment on the relationship between pre- and postsynaptic potentials. *J. Neurobiol.* **1**:437–457.

KUSANO, K., D. R. LIVENGOOD, and R. WERMAN. 1967. Correlation of transmitter release with membrane properties of the presynaptic fiber of the squid giant synapse. *J. Gen. Physiol.* **50**:2579–2601.

LESTER, H. A. 1970. Transmitter release by presynaptic impulses in the squid stellate ganglion. *Nature (Lond.).* **227**:493–496.

LLINÁS, R. R. 1977. Calcium and transmitter release in squid synapse. *Soc. Neurosci. Symp.* **20**:139–160.

LLINÁS, R. 1979. The role of calcium in neuronal function. *In* The Neurosciences: Fourth Study Program. F. O. Schmitt, and F. G. Worden, editors. M.I.T. Press, Cambridge, Mass. 555–571.

LLINÁS, R., and J. R. HEUSER. 1977. Depolarization-release coupling systems in neurons. *Neurosci. Res. Prog. Bull.* **15**:557–687.

LLINÁS, R., and C. NICHOLSON. 1975. Calcium role in depolarization-secretion coupling: an aequorin study in squid giant synapse. *Proc. Natl. Acad. Sci. U.S.A.* **72**:187–190.

LLINÁS, R., I. Z. STEINBERG, and K. WALTON. 1976. Presynaptic calcium currents, and their relation to synaptic transmission: voltage clamp study in squid giant synapse, and theoretical model for the calcium gate. *Proc. Natl. Acad. Sci. U.S.A.* **73**:2918–2922.

LLINÁS, R., I. Z. STEINBERG, and K. WALTON. 1979. A model for synaptic transmission. *Brain Res. Bull.* **4**:170–173.

LLINÁS, R., I. Z. STEINBERG, and K. WALTON. 1981. Relationship between presynaptic calcium current and postsynaptic potential in squid giant synapse. *Biophys. J.* **33**:323–352.

LLINÁS, R., and M. SUGIMORI. 1980. Electrophysiological properties of *in vitro* Purkinje cell somata in mammalian cerebellar slices. *J. Physiol. (Lond.).* **305**:171–195.

LLINÁS, R., K. WALTON, and V. BOHR. 1976. Synaptic transmission in squid giant synapse after potassium conductance blockage with external 3- and 4-aminopyridine. *Biophys. J.* **16**:83–86.

LUX, H. D., and C. B. HEYER. 1979. A new electrogenic calcium-potassium system. *In* The Neurosciences: Fourth Study Program. F. O. Schmitt and F. G. Worden, editors. M.I.T. Press, Cambridge, Mass.

MARTIN, A. R., and G. L. RINGHAM. 1975. Synaptic transfer at a vertebrate central nervous system synapse. *J. Physiol. (Lond.).* **251**:409–426.

MAYNARD, D. M., and K. D. WALTON. 1975. Effects of maintained depolarization of presynaptic neurons on inhibitory transmission in lobster neuropil. *J. Comp. Physiol.* **A97**:215–243.

MEECH, R. W. 1978. Calcium-dependent potassium activation in nervous tissues. *Ann. Rev. Biophys. Bioeng.* **7**:1–18.

MEVES, H., and W. VOGEL. 1973. Calcium inward currents in internally perfused giant axons. *J. Physiol. (Lond.).* **235**:225–265.

MILEDI, R. 1973. Transmitter release induced by injection of calcium ions into nerve terminals. *Proc. R. Soc. Lond. B Biol. Sci.* **183**:421–425.

NARAHASHI, T., J. W. MOORE, and W. R. SCOTT. 1964. Tetrodotoxin blockage of sodium conductance increase on lobster giant axons. *J. Gen. Physiol.* **47**:965–974.

NEW, W., and W. TRAUTWEIN. 1972. The ionic nature of slow inward current and its relation to concentration. *Pflugers Arch.* **334**:24–38.

OKAMOTO, H., K. TAKAHASHI, and M. YOSHII. 1976. Two components of the calcium current in the egg cell membrane of the tunicate. *J. Physiol. (Lond.)* **255**:527–561.

PEARSON, K. G. 1979. Local neurons and local interactions in the nervous systems of invertebrates. *In* The Neurosciences: Fourth Study Program. F. O. Schmitt, and F. G. Worden, editors. M.I.T. Press, Cambridge, Mass.

PEARSON, K. G., and C. R. FOURTNER. 1975. Nonspiking interneurons in walking system of the cockroach. *J. Neurophysiol.* **38**: 33–52.

PELHATE, M., and Y. PICHON. 1974. Selective-inhibition of potassium current in giant-axon of cockroach. *J. Physiol. (Lond.).* **242**:P90–91.

PUMPLIN, D. W., and T. S. REESE. 1978. Membrane ultrastructure of the giant synapse of the squid *Loligo pealeii*. *Neuroscience.* 3:685–696.

ROSS, W. N., and A. E. STUART. 1978. Voltage-sensitive calcium channels in the presynaptic terminals of a decrementally conducting photoreceptor. *J. Physiol. (Lond.).* **274**:173–191.

SANCHEZ, J. A., and E. STEFANI. 1978. Inward calcium current in twitch muscle fibres of the frog. *J. Physiol. (Lond.).* **283**:197–209.

SCHWARTZ, T. L., and C. R. HOUSE. 1970. A small-tipped microelectrode designed to minimize capacitative artifacts during the passage of current through the bath. *Rev. Sci. Instrum.* **41**:515–517.

SHAPIRO, E., V. F. CASTELLUCCI, and E. R. KANDEL. 1980. Presynaptic membrane potential affects transmitter release in an identified neuron in *Aplysia* by modulating the Ca^{2+}, and K^+ currents. *Proc. Natl. Acad. Sci. U.S.A.* **77**:629–633.

STANDEN, N. B. 1975. Voltage-clamp studies of the calcium inward current in an identified snail neurone: comparison with the sodium inward current. *J. Physiol. (Lond.).* **249**:253–268.

TAKEUCHI, A., and N. TAKEUCHI. 1962. Electrical changes in pre- and postsynaptic axons of the giant synapse of *Loligo*. *J. Gen. Physiol.* **45**:1181–1193.

YEH, J. Z., G. S. OXFORD, C. H. WU, and T. NARAHASHI. 1976. Dynamics of aminopyridine block of potassium channels in squid axon membrane. *J. Gen. Physiol.* **68**:519–535.

YOUNG, J. Z. 1939. Fused neurones, and synaptic contacts in the giant nerve fibres of cephalopods. *Philos. Trans. R. Soc. Lond. B Biol. Sci.* **229**:465–503.

YOUNG, J. Z. 1973. The giant fibre synapse of *Loligo*. *Brain Res.* **57**:457–460.